HHS Public Access

Author manuscript

Cell Rep. Author manuscript; available in PMC 2021 October 21.

Published in final edited form as:

Cell Rep. 2021 March 23; 34(12): 108893. doi:10.1016/j.celrep.2021.108893.

FoxO1 suppresses Fgf21 during hepatic insulin resistance to impair peripheral glucose utilization and acute cold tolerance

Oliver Stöhr[1], **Rongya Tao**[1], **Ji Miao**[1], **Kyle D. Copps**[1], **Morris F. White**[1,2,*]

[1]Division of Endocrinology, Boston Children's Hospital, Harvard Medical School, Boston, MA 02215, USA

[2]Lead contact

SUMMARY

Fgf21 (fibroblast growth factor 21) is a regulatory hepatokine that, in pharmacologic form, powerfully promotes weight loss and glucose homeostasis. Although "Fgf21 resistance" is inferred from higher plasma Fgf21 levels in insulin-resistant mice and humans, diminished Fgf21 function is understood primarily via *Fgf21* knockout mice. By contrast, we show that modestly reduced Fgf21—owing to cell-autonomous suppression by hepatic FoxO1—contributes to dysregulated metabolism in LDKO mice ($Irs1^{L/L}$·$Irs2^{L/L}$·Cre^{Alb}), a model of severe hepatic insulin resistance caused by deletion of hepatic Irs1 (insulin receptor substrate 1) and Irs2. Knockout of hepatic *Foxo1* in LDKO mice or direct restoration of Fgf21 by adenoviral infection restored glucose utilization by BAT (brown adipose tissue) and skeletal muscle, normalized thermogenic gene expression in LDKO BAT, and corrected acute cold intolerance of LDKO mice. These studies highlight the Fgf21-dependent plasticity and importance of BAT function to metabolic health during hepatic insulin resistance.

In brief

Genetic disruption of hepatic insulin signaling reduces circulating Fgf21, which Stöhr et al. reveal owes to cell-autonomous suppression of Fgf21 by hepatic FoxO1. Lower Fgf21 in this context reversibly alters brown adipose tissue (BAT) gene expression, resulting in impaired glucose utilization, excess lipid accumulation in BAT, and acute cold intolerance.

Graphical Abstract

*Correspondence: morris.white@childrens.harvard.edu.

AUTHOR CONTRIBUTIONS

O.S. designed and performed experiments with support of R.T. and oversight by M.F.W. J.M. provided critical reagents and commentary. K.D.C. and M.F.W. prepared the manuscript with input and approval of all authors.

SUPPLEMENTAL INFORMATION

Supplemental information can be found online at https://doi.org/10.1016/j.celrep.2021.108893.

DECLARATION OF INTERESTS

M.F.W. is an advisory board member of Housey Pharma (https://www.housey.com/).

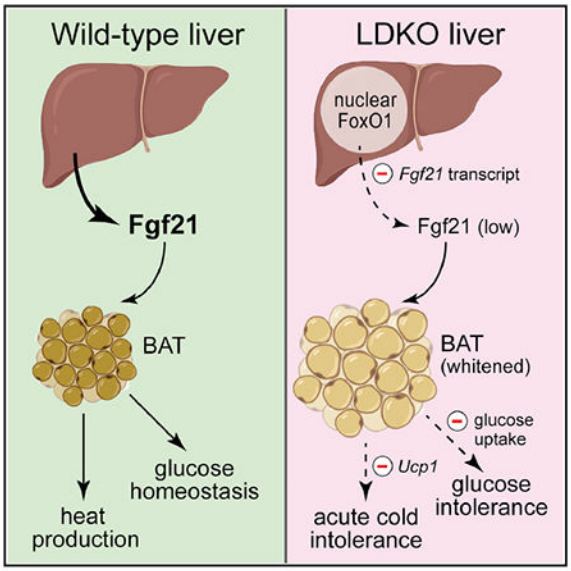

INTRODUCTION

Hepatic insulin resistance contributes to type 2 diabetes and cardiovascular disease through increased hepatic glucose production and lipoprotein secretion (Petersen and Shulman, 2018), as well as dysregulated synthesis and secretion of hepatokines (Stefan and Häring, 2013). Signaling by the insulin receptor (IR), including activation of the phosphatidylinositol 3-kinase (PI3K)→Akt1/2 pathway, is coordinated by insulin receptor substrate 1 (Irs1) and Irs2. We have shown that liver-specific knockout of *Irs1* and *Irs2* in LDKO mice ($Irs1^{L/L}$·$Irs2^{L/L}$·Cre^{Alb}) promotes hepatic glucose production (HGP), glucose intolerance, hyperinsulinemia, and diabetes (Cheng et al., 2009; Dong et al., 2008; Guo et al., 2009; Tao et al., 2018). Remarkably, the WAT (white adipose tissue), BAT (brown adipose tissue), and skeletal muscles of LDKO mice also become insulin resistant, illustrating that dysregulated hepatic metabolism is communicated to these peripheral insulin-sensitive tissues (Tao et al., 2018).

Activation of the hepatic PI3K→Akt1/2 pathway results in the phosphorylation and nuclear exclusion of transcription factor FoxO1 (Forkhead box O1), which up- or downregulates the expression of many genes to coordinate insulin-regulated metabolic homeostasis (Dong et al., 2008). Glycemic effects of hepatic insulin resistance owe to excess FoxO1 activity, as glucose homeostasis is restored to LDKO mice by genetic or viral Cre-mediated deletion of hepatic *Foxo1* in "LTKO" mice (LDKO·$FoxO1^{L/L}$) (Cheng et al., 2009; Dong et al., 2008; Tao et al., 2018). These findings have been confirmed and extended by others using compound hepato-specific IR·FoxO1 knockout or Akt1·Akt2·FoxO1 knockout mice (Lu et al., 2012; O-Sullivan et al., 2015; Perry et al., 2015; Titchenell et al., 2016).

Dysregulated glucose homeostasis in LDKO and similar mice owes in part to impaired suppression of WAT lipolysis, which mediates insulin's "indirect" control of HGP (Fisher and Kahn, 2003; Perry et al., 2015; Roden and Shulman, 2019; Tao et al., 2018). We have shown that impaired WAT anti-lipolysis in LDKO mice owes to increased expression

of FoxO1-induced hepatokine Fst (follistatin) (Tao et al., 2018). However, BAT insulin resistance in LDKO mice appears independent of Fst (Tao et al., 2018). Additional FoxO1-dependent hepatokines might regulate BAT, as up to a quarter of hepatic proteins are secreted into the circulation (Meex and Watt, 2017), including Fgf21 (fibroblast growth factor 21), AHSG (fetuin), selenoprotein P13, SHBG (sex hormone-binding globulin), and adropin (Li et al., 2016; Michos et al., 2008; Stefan and Häring, 2013; Tao et al., 2018; Yang et al., 2011; Zhao et al., 2015).

Fgf21 is a member of the endocrine family of FGFs that lack heparin-binding capacity, facilitating its entry into the circulation (Beenken and Mohammadi, 2009). Though Fgf21 is expressed in other tissues, under normal physiologic conditions, circulating Fgf21 comes from the liver (Markan et al., 2014). Fgf21 binds to a receptor complex composed of an FGF receptor (Fgfr) and β-Klotho (Klb) (Kuro, 2018). Knockout and antibody studies show that Fgfr1c·Klb mediate the bulk of Fgf21 actions in mice (Adams et al., 2012; Kliewer and Mangelsdorf, 2019); however, hepatocytes are thought to respond poorly to physiologic Fgf21, as they mainly express Fgfr4·Klb (Yang et al., 2012). Thus, circulating Fgf21 acts largely to transmit hepatic metabolic status to the fat, nervous, and other tissues (Kliewer and Mangelsdorf, 2019).

Hepatic Pparα (peroxisome proliferator activated receptor alpha)—acting in combination with Nupr1 (nuclear protein transcription regulator 1) and Atf4 (activating transcription factor 4) or Chrebp (carbohydrate response element binding protein)—upregulates *Fgf21* expression in response to fasting, protein deficiency, or carbohydrate excess to enhance insulin sensitivity during refeeding, promote energy expenditure in BAT, and suppress sweet preference (BonDurant and Potthoff, 2018). In mice, knockout of hepatic *Fgf21* specifically impairs glucose uptake into BAT (Markan et al., 2014), and the acute glucose-lowering effect of pharmacologic Fgf21 is abolished by disruption of BAT Fgf21 signaling (BonDurant et al., 2017). Importantly, Pparα induction of hepatic Fgf21 during early post-natal development is required for BAT thermogenic gene expression and function in mice (Hondares et al., 2010). Moreover, genes mediating glucose uptake, fatty acid oxidation, and uncoupled respiration in BAT–such as *Slc2a1* (Glut1), *Cpt1a*, and *Ucp1*–can be upregulated in adult mice by the administration of exogenous Fgf21 (Fisher et al., 2012; Kharitonenkov et al., 2005). Compatible with these findings, liver-derived Fgf21–rather than Fgf21 from adipose or other tissues–is required for body temperature maintenance in acutely cold-exposed mice (Ameka et al., 2019).

Circulating Fgf21 concentration in healthy mice or humans is highest during fasting or exercise, when insulin:glucagon ratios are low (Hansen et al., 2015). Whereas circulating Fgf21 is typically elevated in insulin-resistant mice or human subjects (Staiger et al., 2017), we show herein that hepato-specific insulin resistance in LDKO mice reduces Fgf21 gene expression and secretion in a hepatic FoxO1-dependent manner, resulting in dysregulated gene expression, impaired glucose uptake and WAT-like lipid accumulation in BAT, and acute cold intolerance of LDKO mice.

RESULTS

Hepatic FoxO1 in LDKO mice dysregulates peripheral glucose utilization in a tissue-specific manner

As described previously, fasted LDKO mice, but not LTKO mice (LDKO·FoxO1$^{L/L}$·Cre^{Alb}) displayed glucose intolerance during an intraperitoneal (i.p.) GTT (glucose tolerance test) and relative insulin resistance by i.p. ITT (insulin tolerance test) (Figures 1A and 1B; Dong et al., 2008). Our previous work suggested that impaired glucose homeostasis in LDKO mice owes at least in part to WAT insulin resistance and excess lipolysis owing to increased expression and secretion of hepatic Fst (Tao et al., 2018). Regardless, the expression of hundreds of hepatic genes is normalized upon deletion of *Foxo1* in the LTKO liver–allowing that additional hepatokines might contribute to the regulation of insulin sensitivity in peripheral tissues (Dong et al., 2008; Tao et al., 2018).

To determine the precise effects of hepatic insulin resistance on peripheral glucose utilization, we measured basal and insulin-stimulated [^{14}C]2DOG (2-deoxyglucose) uptake into WAT, BAT, and skeletal muscle of control (CTRL), LDKO, and LTKO mice. Unexpectedly, [^{14}C]2DOG uptake by eWAT (epigonadal WAT) and iWAT (inguinal WAT) in LDKO mice was equivalent to that in CTRL or LTKO mice (Figures 1C and 1D). By contrast, both basal and insulin-stimulated [^{14}C]2DOG uptake into BAT of LDKO mice were reduced significantly compared against CTRL or LTKO mice (Figure 1E). Moreover, insulin-stimulated [^{14}C]2DOG uptake into skeletal muscle–taken as the aggregate uptake by quadriceps, gastrocnemius, soleus, tibialis anterior, and extensor digitorum longus–was similarly impaired in LDKO mice (Figure 1F). Thus, peripheral glucose disposal in LDKO mice is dysregulated in a tissue-specific and hepatic FoxO1-dependent fashion.

Hepatic FoxO1 in LDKO mice promotes lipid accumulation in BAT

To investigate effects of differential glucose uptake by peripheral tissues, we employed DEXA (dual X-ray absorptiometry) to determine the body composition of 24-week-old CTRL, LDKO, and LTKO mice fed a chow diet (CD). Owing to previously described dysregulation of hepatic growth hormone response and insulin growth factor 1 (IGF1) production (Dong et al., 2008), LDKO mice weighed around 20% less than CTRL mice ($p < 0.0001$), whereas LTKO mice weighed only 2% less (not significant; Figure 1G). Compared against CTRL mice, overall adiposity (% fat mass) was about 7% lower in LDKO ($p < 0.0001$) and around 5% lower in LTKO mice ($p < 0.01$), with correspondingly minor increases in lean body composition (% lean mass; Figures 1H and 1I). Using separate groups of adult LDKO and LTKO mice and their respective controls, we carefully measured the individual masses of eWAT and iWAT depots but identified only a trend toward reduced eWAT mass in LDKO mice ($p = 0.0501$; Figure S1A). Regardless, examination of their similarly sized iWAT depots revealed that the average size of individual adipocytes in iWAT of LDKO or LTKO mice was about 50% larger than in CTRL mice ($p < 0.01$ or $p < 0.05$, respectively; Figures S1B and S1C).

By comparison with eWAT or iWAT depots, the interscapular BAT mass in LDKO mice was abnormally light (or white) in color and about 2-fold more massive than in Irs1$^{L/L}$·Irs2$^{L/L}$

controls ($p < 0.001$; median: 153 mg versus 73 mg); by contrast, BAT mass was comparable between LTKO mice and controls ($Irs1^{L/L}$·$Irs2^{L/L}$·$FoxO1^{L/L}$; Figure 1J). At the cellular level, H&E staining and morphometry revealed comparably sized brown adipocytes in CTRL and LTKO BAT but around 6.5-fold-enlarged brown adipocytes in LDKO BAT ($p < 0.01$) with unilocular lipid droplets more typical of WAT adipocytes (Figures 1K, 1L, and S1D). Thus, the presence of unrestrained hepatic FoxO1 activity during complete hepatic insulin resistance (LDKO mice) moderately reduced WAT adiposity, although promoting triglyceride accumulation in BAT.

Correction of hepatic Fgf21 insufficiency in LDKO mice normalizes BAT and muscle glucose uptake and restores peripheral insulin sensitivity

The uncoupled oxidation of glucose and fatty acids in BAT provides an important defense against obesity and metabolic disease (Chartoumpekis et al., 2011; Chondronikola et al., 2014; Peres Valgas da Silva et al., 2019). Although glucose uptake into BAT of LDKO mice was impaired (Figure 1E), we previously observed that hepatic overexpression and hyper-secretion of Fst did not affect BAT glucose disposal in wild-type mice (Tao et al., 2018). Therefore, we queried the list of FoxO1-regulated genes in the LDKO liver (Tao et al., 2018) to identify secreted proteins that might promote BAT lipid accumulation during hepatic insulin resistance. Fgf21–for which we observed lower mRNA expression in LDKO liver by array hybridization (Tao et al., 2018)–was selected for study, owing to its known function as a hepatokine regulating BAT function and lipid oxidation (BonDurant et al., 2017; BonDurant and Potthoff, 2018; Fisher et al., 2012; Kharitonenkov et al., 2005; Markan et al., 2014). Quantitative PCR confirmed that hepatic *Fgf21* mRNA in fasted LDKO mice was around half that in CTRL or LTKO mice–a reduction like that previously described in mice lacking hepatic insulin receptors (Emanuelli et al., 2014; Ling et al., 2018; Figure 2A). Hepatic Fgf21 mRNA moreover remained significantly lower in LDKO mice that were fasted and then allowed to refeed for 4 h (Figure S2A). Compatible with suppression of hepatic *Fgf21* by FoxO1, plasma Fgf21 in LDKO mice was only 34% of that in CTRL mice ($p < 0.0001$), whereas Fgf21 in LTKO mice was within the low normal range (74% of CTRL mean; $p < 0.05$; Figure 2B).

Because Fgf21 in mice reduces blood glucose and lipids at least in part through its effects on BAT, we hypothesized that restoring Fgf21 might re-establish systemic glucose homeostasis in LDKO mice. Thus, we infected livers of control and LDKO mice with $Fgf21^{AdV}$ (adenovirus expressing murine Fgf21) or GFP^{AdV} (control virus expressing green fluorescent protein). Infection with $Fgf21^{AdV}$ significantly increased *Fgf21* mRNA concentration in liver, but not BAT, iWAT, eWAT, or skeletal muscle of LDKO mice (Figure S2B). By 12 days after infection, circulating Fgf21 in LDKO·$Fgf21^{AdV}$ mice increased significantly (versus LDKO·GFP^{AdV} mice) to about 1.5-fold of the level in CTRL·GFP^{AdV} mice (Figure 2C). Glucose tolerance in LDKO·$Fgf21^{AdV}$ mice improved significantly in comparison with LDKO·GFP^{AdV} mice–but remained slightly impaired relative to CTRL·GFP^{AdV} mice (Figure 2D). Regardless, $Fgf21^{AdV}$ infection completely normalized insulin tolerance in LDKO mice (Figure 2E). As expected from their restored insulin sensitivity, fasting serum insulin in LDKO·$Fgf21^{AdV}$ mice decreased by 3.2-fold compared against LDKO·GFP^{AdV} mice ($p < 0.0001$) but remained above the normal

level in CTRL·GFP^{AdV} mice ($p < 0.01$; Figure 2F). In contrast with published data from mice lacking hepatic insulin receptors and reconstituted with Fgf21 (Emanuelli et al., 2014), LDKO mice infected with Fgf21^{AdV} also showed significantly reduced glucose excursion after injection with the gluconeogenic precursor pyruvate (PTT) (Figure 2G). However, as LDKO mice are well validated to lack hepatic insulin signaling (Dong et al., 2008), improved pyruvate tolerance in LDKO·Fgf21^{AdV} mice most likely owed to greater peripheral glucose disposal rather than suppressed HGP. Supporting this conclusion, infection with Fgf21^{AdV} reduced glucose excursion during PTT by just 19% in LDKO·Fgf21^{AdV} mice but by 41% in CTRL·Fgf21^{AdV} mice (dash line, Figure 2G).

To directly measure the effects of Fgf21^{AdV} on glucose utilization by peripheral tissues, we measured *in vivo* uptake of [^{14}C] 2DOG. Consistent with our earlier observations (Figures 1C and 1D), CTRL and LDKO mice infected with GFP^{AdV} manifested similar glucose uptake into eWAT and iWAT depots (Figures 2H and 2I), although insulin-stimulated uptake into iWAT was mildly increased in LDKO·Fgf21^{AdV} versus LDKO·GFP^{AdV} mice (Figure 2I). In contrast, infection with Fgf21^{AdV} completely normalized insulin-stimulated [^{14}C]2DOG uptake into BAT of LDKO mice (Figure 2J). Consistent with this result, impaired expression of genes encoding glucose transporters Glut1 and Glut4 in LDKO BAT was either completely normalized (Glut1) or significantly improved (Glut4) by infection with Fgf21^{AdV} (Figure 2K). Additionally, basal and insulin-stimulated [^{14}C]2DOG uptake into hind-limb skeletal muscles of LDKO·Fgf21^{AdV} mice increased into the normal range established by CTRL·GFP^{AdV} mice (Figure 2L). Thus, alleviation of the circulating Fgf21 deficiency in LDKO mice by Fgf21^{AdV} infection of the liver was sufficient to normalize BAT and muscle glucose uptake, together with glucose tolerance.

Normalized Fgf21 expression maintains glucose homeostasis in LTKO mice

Although hepatic *Foxo1* deletion incompletely restored Fgf21 in LTKO mice, relative to control mice (Figure 2B), we hypothesized that this partial restoration was enough to improve metabolic health in LTKO mice (Dong et al., 2008; Tao et al., 2018). Thus, we infected LTKO mice with a short hairpin-expressing virus to knock down hepatic *Fgf21* (shFgf21^{AdV}) or control virus expressing a scrambled, non-targeting RNA sequence (scRNA^{AdV}). Infection with shFgf21^{AdV} significantly reduced *Fgf21* mRNA concentration in liver, but not BAT, iWAT, eWAT, or skeletal muscle of LTKO mice (Figure S3A). In LTKO·shFgf21^{AdV} mice—but not in control LTKO·scRNA^{AdV} mice–circulating Fgf21 decreased to approximately the level in LDKO mice (Figure 3A). To gauge the impact of this reduction, we measured glucose tolerance and insulin sensitivity in GTT and ITT assays. Both glucose tolerance and insulin sensitivity were significantly impaired in LTKO·shFgf21^{AdV} mice versus scRNA^{AdV}-infected controls–to the point that LTKO·shFgf21^{AdV} mice strongly resembled (GTT) or were not significantly different (ITT) from LDKO mice (Figures 3B and 3C). As expected from our analysis of glucose utilization in LDKO mice (Figures 1C–1F), insulin-stimulated uptake of [^{14}C]2DOG into BAT and skeletal muscles of LTKO·shFgf21^{AdV} mice was significantly impaired versus that in uninfected or scRNA^{AdV}-infected LTKO mice (Figures 3D and 3E). Thus, we conclude that higher *Fgf21* expression, relative to LDKO mice, is important for improved glucose homeostasis in LTKO mice.

FoxO1 regulates hepatic *Fgf21* expression in a cell-autonomous fashion

Because dietary or metabolic factors, more than insulin itself, have been described to determine circulating Fgf21 concentration, we investigated the basis of Fgf21 insufficiency in LDKO mice. Higher glycemia appeared to be ruled out as a cause, because this is associated with increased *Fgf21* transcription, at least acutely (BonDurant and Potthoff, 2018). Fatty acids, acting through transcriptional activator PPARα, can promote hepatic *Fgf21* expression in both mice and humans (Badman et al., 2007; Fisher and Maratos-Flier, 2016; Hondares et al., 2010; Inagaki et al., 2007). Moreover, serum-free fatty acids that might include or be metabolized to PPARα ligands are low in fasted LDKO mice (Dong et al., 2008). However, in published microarray data from fasted LDKO and LTKO mice (Dong et al., 2008), we found that *Fgf21* was strongly downregulated relative to more than 20 other known or potential PPARα target genes in the LDKO liver (Figure 3F). In contrast, *Fgf21* expression in LTKO liver was higher than in CTRL liver although the expression of many PPAR· target genes upregulated in LDKO liver (such as *Cd36*) was decreased (Figure 3F).

It was previously shown that liver-specific *Foxo1* knockout mice have higher hepatic *Fgf21* mRNA and circulating Fgf21 (Haeusler et al., 2010). However, it was not shown whether this owed to direct or indirect effects of nuclear FoxO1 or to cell-nonautonomous effects of overexpressed FoxO1. To address this question, we infected mouse primary hepatocytes with $Foxo1^{AdV}$ to augment *Foxo1* expression or with $shFoxo1^{AdV}$to knock down *Foxo1*. As controls, we infected hepatocytes with GFP^{AdV} or $scRNA^{AdV}$ (respectively). As *Foxo1* and *Fgf21* expression were insensitive to infection with control viruses (Figures 3G and S3B, open bars), we used the average expression in these infections as a synthetic control group.

Infection of primary hepatocytes with $Foxo1^{AdV}$ or $shFoxo1^{AdV}$ dose-dependently increased or decreased *Foxo1* mRNA (Figure S3B). Conversely, infection with $Foxo1^{AdV}$ significantly reduced hepatocyte *Fgf21* expression, whereas $shFoxo1^{AdV}$ infection significantly increased *Fgf21* mRNA (Figure 3G); as both viruses dose-dependently affected *Fgf21,* the expected linear trend in *Fgf21* expression was also highly significant ($p < 0.0001$). Regardless, even high-dose $Foxo1^{AdV}$ suppressed *Fgf21* expression by only around 55%. Because the murine *Fgf21* promoter lacks canonical elements that mediate FoxO1 binding–and published chromatin immunoprecipitation experiments have not identified *Fgf21* as a FoxO1-regulated gene (Shin et al., 2012)–we conclude that FoxO1 regulated *Fgf21* in a hepatocyte-autonomous but likely indirect manner.

HFD-induced upregulation of Fgf21 fails to improve glucose homeostasis in LDKO mice

In wild-type mice, metabolic stress caused by feeding a HFD (high-fat diet) increases circulating Fgf21 (Staiger et al., 2017). To gauge the maintenance and importance of this regulation in the face of hepatic insulin resistance, we compared CTRL, LDKO, and LTKO mice that were fed a standard CD or HFD (60% kcal from fat). After 16 weeks on HFD, CTRL and LTKO mice each became overweight (48.2 g versus 43.1 g; $p = 0.838$), whereas LDKO mice grew only slightly heavier than CD-fed LDKO mice of the same age (29.6 g versus 26.9 g; $p = 0.275$; Figure 4A; data not shown). Although LDKO mice are growth impaired from birth (Dong et al., 2008), the reduced weight gain of HFD-fed LDKO mice owed largely to reduced fat accumulation, as overall adiposity (percent fat mass or absolute

fat mass) was significantly lower in LDKO mice than in CTRL or LTKO mice (Figures 4B and S4A). In contrast, percent lean body mass was significantly higher in LDKO mice than in CTRL or LTKO mice, even though absolute lean mass was somewhat lower (Figures S4B and S4C).

Measurement of serum Fgf21 after 10 weeks on HFD or CD identified a significant effect of HFD to increase circulating Fgf21 in CTRL, LDKO, and LTKO mice; yet Fgf21 remained lowest in LDKO mice, regardless of diet (Figure 4C). Increased circulating Fgf21 in the context of HFD feeding was not enough to improve glucose tolerance or insulin sensitivity, even in the less-obese and normally Fgf21-insufficient LDKO mice (Figures 4D and 4E). In line with their decreased obesity, BAT [^{14}C] 2DOG uptake in LDKO mice was less negatively impacted by HFD consumption than in CTRL mice (Figure 4F). However, as the rate of insulin-stimulated [^{14}C]2DOG uptake remained 26% lower in LDKO than in CTRL mice on HFD ($p = 0.058$; Figure 4F), we conclude that metabolic stress produced by HFD feeding was dominant over upregulation of Fgf21 in determining systemic glucose homeostasis in LDKO mice.

Hepatic Irs1 and Irs2 are dispensable for the weight and glucose-reducing effects of Fgf21 in HFD-fed mice

Previously, it was reported that hepatic insulin receptor expression is not required for the weight and glucose-reducing effects of exogenous (pharmacologic) Fgf21 (Emanuelli et al., 2014). To confirm that hepatic insulin receptor substrates are, likewise, not required, we fed HFD to small groups of CTRL and LDKO mice and infected these after 25 days with GFP^{AdV} or Fgf21^{AdV}. Although body weights of the HFD-fed mice differed dramatically at the time of infection, infection of CTRL and LDKO mice with Fgf21^{AdV} produced nearly equivalent relative weight loss (−26% versus −27%) within 15–20 days (Figure 4G). Similarly, hyperglycemia in both HFD-fed CTRL and LDKO mice was dramatically and stably reduced to around 100 mg/dL from day 26 through at least day 60 (Figure 4H). Measurement of basal and insulin-stimulated [^{14}C]2DOG uptake in CTRL·Fgf21^{AdV} and LDKO·Fgf21^{AdV} mice revealed statistically indistinguishable uptake into BAT, skeletal muscles, eWAT, or iWAT (Figures 4I and S4D–S4F). Moreover, both CTRL·Fgf21^{AdV} and LDKO·Fgf21^{AdV} mice showed improved glucose tolerance and insulin sensitivity relative to their GFP^{AdV}-infected peers (Figures 4J and 4K). However, glucose tolerance remained significantly impaired in LDKO·Fgf21^{AdV} mice versus CTRL·Fgf21^{AdV} mice (Figure 4J); this likely owed to persistent unsuppressed HGP in the HFD-fed LDKO·Fgf21^{AdV} mice, as indicated by their more-profound blood glucose excursion following injection with the gluconeogenic precursor pyruvate (Figure 4L).

Considering that Fgf21 promotes the clearance of hepatic lipid, we also measured hepatic triglyceride (TG) content in CTRL and LDKO mice that were infected with GFP^{AdV} or Fgf21^{AdV}. As background, we first confirmed that hepatic TG content was moderately higher in LDKO than in CTRL mice fed CD, as previously reported (Figure S4G; Dong et al., 2008). In contrast, hepatic TG in HFD-fed mice correlated with their degree of obesity, as demonstrated by lower hepatic TG content in LDKO·GFP^{AdV} mice than in CTRL·GFP^{AdV} mice ($p < 0.01$; Figure S4H). Thus, although Fgf21^{AdV}

infection insignificantly reduced already low hepatic TG in LDKO mice, it resulted in equivalent hepatic TG content in CTRL·Fgf21^{AdV} and LDKO·Fgf21^{AdV} mice (Figure S4H). Collectively, these data demonstrate that hepatic Irs1 and Irs2 are not required for the weight loss and gluco-regulatory effects of exogenous Fgf21 in HFD-fed mice but are required for suppression of HGP, as well as effective hepatic lipid clearance by exogenous Fgf21.

The expression of β-oxidation and thermogenic genes is impaired in BAT of LDKO mice

Fgf21 insufficiency in LDKO mice–or in LTKO mice following *Fgf21* knockdown (LTKO·shFgf21^{AdV} mice)–significantly impaired glucose uptake into BAT (Figures 1E and 3D). To identify related effects of hepatic insulin resistance on BAT function in LDKO, we measured the BAT expression of marker genes characteristic of BAT, skeletal muscle, or WAT, as well as BAT genes involved in β-oxidation of fatty acids and thermogenesis. Compared against CTRL tissue, the aggregate expression of BAT marker genes in LDKO BAT was generally lower (6 of 7 genes tested), with *Eva1* (a.k.a. *Mpzl2* [myelin protein zero-like 2]) displaying the most significant decrease ($p < 0.05$; Figure 5A). Moreover, the expression of genes involved in β-oxidation of fatty acids–such as *Ppara* (PPARα), *Ppara* (PPARγ), *Cpt1a* (carnitine palmitoyltransferase 1a), *Esrra* (estrogen-related receptor α), and *Mcad* (medium-chain acyl-coenzyme A [CoA] dehydrogenase)–was significantly reduced in BAT of LDKO mice, along with that of key thermogenic genes (Figure 5A).

Among thermogenic genes we assayed, *Ucp1* (uncoupling protein 1) and *Prdm16* (PR domain-containing 16) were each expressed at a significantly lower level in LDKO BAT ($p < 0.01$ and $p < 0.05$, respectively; Figure 5A). Whereas Ucp1 directly mediates mitochondrial uncoupling in brown adipocytes, Prdm16 is a transcription factor that regulates the thermogenic gene expression program in brown and beige adipocytes and controls a bidirectional cell fate switch between skeletal myoblasts and BAT (Harms et al., 2014; Seale et al., 2008). Consistent with lower *Prdm16* expression in LDKO BAT, the aggregate expression of skeletal muscle marker genes was higher–especially *Myh7* (myosin heavy chain β) ($p < 0.01$; Figure 5A). More strikingly, BAT from LDKO mice displayed higher aggregate expression of WAT marker genes (Schoettl et al., 2018; $p < 0.0001$)–including *En1, Vdr, Gpc4, HoxC8, HoxA5, Thbd,* and *Nr2f1* (Figure 5A). These results were consistent with reduced β-oxidation of fatty acids in LDKO BAT implied by the accumulation of large, unilocular lipid droplets characteristic of mature WAT (Rosen and Spiegelman, 2006; see Figures 1K and 1L).

Cold intolerance and dysregulated BAT gene expression in LDKO mice are alleviated by restoration of hepatic Fgf21 expression

In mammals exposed to cold temperature, BAT mediates nonshivering thermogenesis within minutes when the sympathetic nervous system (SNS) activates β-adrenergic receptor (βAR) signaling to increase fuel uptake and oxidation for heat generation by Ucp1 (Cannon and Nedergaard, 2011; Nedergaard et al., 2001; Townsend and Tseng, 2014). Because genes that promote β-oxidation and mitochondrial uncoupling are expressed at lower levels in LDKO BAT, and the brown adipocytes accumulate lipid in LDKO mice, we used implanted probes to measure the effect of decreasing ambient temperature upon core body temperature (T^{Core}) in CTRL and LDKO mice. The mice, at initial T^{Core} of 35.5°C, were placed into

metabolic cages for 12 h, during which the ambient temperature decreased linearly to 4°C during the first 2 h. The rate of decline in T^{Core} ($-dT^{Core}$) in LDKO mice over the first 3 h was approximately 2-fold that in CTRL mice ($p = 0.047$), resulting in moderately lower T^{Core} at the 3-h point (−0.45°C; not significant); however, over the next 9 h, T^{Core} in LDKO mice remained around 34.0°C, whereas T^{Core} in CTRL mice recovered to as high as 35.4°C before falling slightly in the last few hours ($p < 0.01$ for area under 12-h T^{Core} curve; Figure 5B). Thus, cold-induced thermogenesis was impaired in LDKO mice, in line with dysregulated BAT gene expression.

To validate the role of hepatic FoxO1 in impaired cold tolerance of LDKO mice, we compared the body temperature of LDKO mice relative to CTRL and LTKO mice during acute 2-h exposure to 4°C. The mice in each group began the experiment with nearly identical T^{Core} (CTRL = 36.46°C; LDKO = 36.66°C; LTKO = 36.35°C; $p = 0.373$); however, T^{Core} in LDKO mice declined twice as rapidly as in CTRL or LTKO mice ($p < 0.001$; Figures 5C and 5E). At the molecular level, we confirmed by qPCR that *Ucp1* expression in BAT was abnormally low in LDKO mice but in the normal range in LTKO mice (Figure 5I), further illustrating the negative effect of hepatic FoxO1 activity upon BAT thermogenic function.

Given that circulating Fgf21 correlates inversely with hepatic FoxO1 activity (Figures 2B and 3A), we tested whether $Fgf21^{AdV}$ could restore cold-induced thermogenesis in adult LDKO mice. During an acute 2-h cold challenge performed 12 days after adenovirus infection, the rate of decline in T^{Core} of LDKO·$Fgf21^{AdV}$ mice was significantly less than in LDKO·GFP^{AdV} mice ($p < 0.01$) and was indistinguishable from that in CTRL·GFP^{AdV} mice (Figures 5D and 5F). In line with these data, BAT *Ucp1* expression was restored to just above the normal range in LDKO·$Fgf21^{AdV}$ mice but remained abnormally low in LDKO·GFP^{AdV} mice (Figure 5J; *Ucp1* data detailed in Figure S5A). Moreover, we found that $Fgf21^{AdV}$ restored the expression of several other β-oxidation and thermogenic genes downregulated in LDKO BAT, including *Ppara, Pparg, Esrra, Pgc1a*, and *Cidea* (Figure 5J). Conversely, $Fgf21^{AdV}$ infection reduced the aberrantly high expression of numerous WAT marker genes in LDKO BAT, particularly *Gpc4, Hoxa5*, and *Thbd* (Figure 5K). Related to these changes in BAT, infection of LDKO mice with $Fgf21^{AdV}$ also augmented the expression of thermogenic genes *Ucp1*, *Pgc1a, Prdm16*, and *Cidea* in iWAT, the site of physiologic cold-induced white adipocyte beigeing (Figure S5B). However, as glucose uptake and thermogenic gene expression were equivalent in iWAT of GFP^{AdV}-infected CTRL and LDKO mice (Figures 1D and S5B)–and thus not correlated with cold tolerance–we conclude that the phenomenon of acute cold intolerance in LDKO mice owes, in large part, to the effects of reduced circulating Fgf21 on BAT gene expression and thermogenic function.

Mechanistically, cold-induced thermogenesis relies upon uncoupled oxidation of available glucose or of fatty acids released from adipocytes as a result of sympathetic nervous activation (Townsend and Tseng, 2014). To isolate and gauge the downstream response to adrenergic activation in LDKO mice, we treated CTRL, LDKO, and LTKO mice with CL316,243–a highly specific β3-adrenoreceptor agonist that increases lipolysis and β-oxidation for heat production (Cannon and Nedergaard, 2004; Yoshida et al., 1996).

Mice were injected i.p. with CL316,243 or vehicle 1 h before exposure to 4°C for 2 h. During the cold challenge, CTRL and LTKO mice displayed identical rates of decline in T^{Core} ($-dT^{Core}$), which treatment with 2 mg/mL CL316,243 reduced by around 40% (Figure 5G; T^{Core} plots in Figure S5C). By contrast, the rate of decline in T^{Core} was 45% greater in LDKO than in CTRL mice, and this more rapid fall in body temperature was not alleviated by treatment with either 1 or 2 mg/mL CL316,243 (Figure 5H; T^{Core} plots in Figure S5D). Compatible with an intact upstream response to CL316,243, the expression of β3 adrenergic receptors was unchanged in BAT of LDKO mice relative to CTRL or LTKO mice (Figure S5E). Thus, bearing in mind the coincident restoration of cold tolerance and BAT thermogenic gene expression in LDKO·$Fgf21^{AdV}$ mice (Figures 5D and 5J), we infer that dysregulated BAT gene expression in LDKO mice likely precludes oxidative and thermogenic use of lipid mobilized by acute adrenergic activation.

DISCUSSION

Interest in the propagation of hepatic insulin resistance to peripheral tissues in LDKO mice led us previously to investigate insulin-regulated hepatokines, including Fst, which is upregulated in the LDKO liver (Tao et al., 2018). Although hepatic Fst overexpression impairs insulin signaling and/or glucose uptake into WAT and skeletal muscles of high-fat-fed mice, it leaves intact glucose disposal into BAT (Tao et al., 2018). Herein, we show that impaired glucose uptake into LDKO BAT associates with an increase in BAT mass and enlarged unilocular fat droplets in brown adipocytes. These alterations occur despite reduced overall adiposity of LDKO mice relative to controls. We further show that rates of insulin-stimulated glucose uptake into WAT depots in LDKO mice are normal, whereas skeletal muscle glucose uptake is impaired. The observation of normal WAT glucose uptake in LDKO mice is counter-intuitive, as we previously showed that insulin signaling in LDKO WAT (estimated by Irs1·PI3K interaction or Akt phosphorylation) is significantly impaired (Tao et al., 2018). Potentially rectifying these observations, it has been shown by others that insulin-stimulated glucose uptake into WAT is at least partially PI3K independent (Liu et al., 2003, 2016) and is surprisingly insensitive to reduced Akt phosphorylation (Czech, 2017; Tan et al., 2015). In any case, we find that glucose disposal into BAT and skeletal muscle—rather than eWAT or iWAT—correlates best with glucose tolerance and insulin sensitivity of LDKO mice.

Previously, it was shown that liver-specific ablation of FoxO1 increases hepatic Fgf21 expression and secretion (Haeusler et al., 2010). Conversely, we and others have shown that LDKO mice or mice lacking hepatic insulin receptors have diminished liver *Fgf21* expression (Dong et al., 2008; Emanuelli et al., 2014) but that this is restored to near normal by genetic ablation of hepatic FoxO1 (Dong et al., 2008; Ling et al., 2018). The regulation of some hepatic genes by FoxO1 may be an indirect result of altered metabolism, as supported by FoxO1's apparently cell-non-autonomous regulation of hepatokine Serpinb1 (El Ouaamari et al., 2019). In contrast, our demonstration that FoxO1 overexpression or knockdown in primary hepatocytes down- or upregulates (respectively) the expression of *Fgf21* strongly supports that hepatic FoxO1 represses *Fgf21* in a cell-autonomous fashion. Nevertheless, because we know of no experimental or informatic evidence supporting direct

association of FoxO1 with the *Fgf21* promoter, we infer that hepatic FoxO1 might indirectly regulate *Fgf21* transcription within hepatocytes.

Potentially, FoxO1 could upregulate a repressor of *Fgf21* transcription or else downregulate an activator. Concerning the latter possibility, effects of hepatic FoxO1 on PPARα and ChREBP are of interest. Overexpression of constitutively nuclear FoxO1 in mouse liver was reported to reduce the expression of PPARα (Matsumoto et al., 2006). However, we and others have observed normal *Ppara* expression in liver of LDKO mice (Dong et al., 2008) or of similar mice lacking hepatic insulin receptors (LIRKO mice; Ling et al., 2018). Moreover, both LDKO and LIRKO mice show increased expression of PPARα target genes, such as *Cd36* (this work; Ling et al., 2018). In contrast to PPARα, the active nuclear form of ChREBP and expression of its specific target *Pklr* are reportedly diminished in LIRKO mouse liver (Haas et al., 2012). There is, moreover, some evidence that diminished *Pklr* expression during severe hepatic insulin resistance owes to FoxO1-mediated downregulation of ChREBP glycosylation by OGT (O-linked N-acetylglucosamine transferase) (Ido-Kitamura et al., 2012); however, the mechanism by which FoxO1 impairs OGT activity is unknown. We conclude that additional FoxO1-regulated factors might contribute directly to *Fgf21* downregulation in the LDKO liver.

We find that plasma Fgf21 concentration in LDKO mice is reduced to around one-third of normal and that its restoration–by either hepatic *Foxo1* deletion in LTKO mice or $Fgf21^{AdV}$ infection of LDKO mice–normalizes insulin-stimulated glucose uptake into BAT and skeletal muscle. The Fgf21 dependence of BAT glucose uptake in LDKO mice is consistent with the described impairment of BAT glucose disposal in liver-specific *Fgf21* knockout mice (Markan et al., 2014). There is also some evidence that Fgf21 promotes glucose uptake into human skeletal muscle (Mashili et al., 2011); however, normalization of muscle glucose uptake in LTKO mice or $Fgf21^{AdV}$-infected LDKO mice might owe to indirect effects of resolved insulin resistance, such as reduced insulinemia.

Given their incomplete Fgf21 insufficiency, it is striking that LDKO mice benefit to such a degree by its restoration. Short-hairpin-mediated knockdown of near-normal hepatic *Fgf21* expression in LTKO mice has similarly profound–but negative–effects, practically reverting BAT and muscle glucose uptake, glucose tolerance, and insulin sensitivity to those of LDKO mice. Thus, LDKO and LTKO mice may highlight a particular sensitivity of glucose homeostasis to BAT function in the context of hepatic insulin resistance. Supporting this idea, dysregulation of metabolic homeostasis in at least one of several systemic *Fgf21* knockout mouse lines ($Fgf21^{tm1Emf}$, produced by Dr. T. Flier) was relatively mild when these mice were fed a CD—manifesting as moderate glucose intolerance, normal insulin tolerance, and a propensity for slight weight gain from increased food intake (Badman et al., 2009). Measurements of serum glucose and insulin concentrations, body weights, and adiposity in other systemic *Fgf21* knockout mouse lines on CD have corroborated these findings (Hotta et al., 2009; Potthoff et al., 2009). By contrast, the same *Fgf21* knockout mice of Flier showed significant glucose intolerance and insulin resistance when fed a HFD, which certainly promotes hepatic insulin resistance (Assini et al., 2015).

Total Fgf21 deficiency has been shown to promote hepatic insulin resistance (Camporez et al., 2015), and hepatic insulin resistance in high-fat-fed wild-type mice or genetically obese mice is ameliorated by pharmacologic Fgf21 (Camporez et al., 2013; Xu et al., 2009a, 2009b). However, combined evidence from LIRKO mice (Emanuelli et al., 2014) and our LDKO mice (herein) does not support a role of hepatic insulin sensitization in Fgf21's beneficial effects upon glucose homeostasis during complete hepatic insulin resistance. First, although we did not extensively survey hepatic gene expression, we found that infection of chow-fed LDKO mice with Fgf21^{AdV} did not reduce high hepatic expression of *Fst*, a FoxO1-upregulated hepatokine (data not shown). Second, echoing Emanuelli et al. (2014), we found using HFD-fed LDKO mice that IR→Irs1/Irs2-mediated hepatic signaling is dispensable for exogenously provided Fgf21 to reduce body weight and normalize glucose homeostasis. Moreover, pyruvate intolerance in LDKO·Fgf21^{AdV} mice supports that excess HGP stemming from loss of hepatic insulin signaling remains no more than partially suppressed by Fgf21 treatment.

Relevant to the effects of diminished circulating Fgf21 upon LDKO BAT, it was shown by others that PPARα-dependent upregulation of hepatic Fgf21 in early life is required for normal BAT expression of genes critical in glucose uptake, fatty acid β-oxidation, and thermogenesis–including *Slc2a1* (Glut1), *Slc2a4* (Glut4), *Pgc1a*, and *Ucp1* (Hondares et al., 2010). These genes comprise a subset of those downregulated in BAT of LKDO mice–the expression of which is reverted toward normal in LTKO and LDKO·Fgf21^{AdV} mice. Compatible with the correction of low body temperature in milk-deprived or PPARα-deficient mouse pups by exogenous Fgf21 (Hondares et al., 2010), we observe intolerance to acute cold in LDKO mice that is corrected in LTKO and LDKO·Fgf21^{AdV} mice. Underlining a specific role of severe hepatic insulin resistance to impair BAT function, dysregulation of BAT gene expression or morphology on par with that in LDKO mice has not, to our knowledge, been described in mice with liver-specific knockout of either *Ppara* or *Fgf21.* However, elevated lipid accumulation was noted previously in brown adipocytes of systemic *Fgf21* knockout mice on a ketogenic diet (Badman et al., 2009).

The details of how liver-derived Fgf21 supports acute cold tolerance deserve continued attention but may well differ between genetically normal mice and those with severe hepatic insulin resistance stemming from gene knockout. Ameka et al. (2019) showed through careful studies that cold-exposed wild-type mice acutely upregulate hepatic Fgf21 secretion and that liver-specific (but not fat-specific) *Fgf21* knockout mice are intolerant of acute cold. Although these authors identified significantly reduced BAT *Ucp1* expression in liver-specific *Fgf21* knockout mice, they reasonably concluded from other experiments using fat-specific *Klb* (β-klotho) knockout mice and measurement of BAT sympathetic nervous activation that the main role of cold-induced hepatic Fgf21 secretion is to augment sympathetic activation (Ameka et al., 2019). Interestingly, we found that treatment of LDKO mice with specific β3AR agonist CL316,243 did not improve acute cold tolerance, even though α3AR expression was normal in LDKO BAT. These results favor that Fgf21^{AdV}-mediated restoration of acute cold tolerance in LDKO mice depends critically upon the upregulation of BAT thermogenic and oxidative genes, which might owe to Fgf21-promoted sympathetic activation. We conclude that BAT in LDKO mice, like that in neonatal pups, remains plastic to Fgf21-mediated gene expression changes and infer by the limited effects

of acute α3AR agonism in LDKO mice that these changes are critical for the restoration of acute cold tolerance.

Whereas circulating Fgf21 is low in LDKO mice, circulating Fst is high (Tao et al., 2018). How dysregulation of Fgf21 integrates with that of Fst to perturb metabolic homeostasis in LDKO mice is of interest, because remedy of either problem largely restores glucose tolerance and insulin sensitivity. Notably, low Fgf21 impairs BAT glucose uptake in LDKO mice and LTKO·shFgf21^{AdV} mice, whereas Fst overexpression does not appear to alter BAT glucose uptake in normal mice (Tao et al., 2018). A further differentiating factor is that restoration of circulating Fgf21 does not correct excessive HGP in LDKO·Fgf21^{AdV} mice, whereas knockdown of high hepatic *Fst* expression in LDKO mice very clearly reduces HGP in hyperinsulinemic-euglycemic clamp studies (Tao et al., 2018). Thus, we conclude that low Fgf21 and high Fst mediate distinct aspects of metabolic dysregulation, owing to severe hepatic insulin resistance, to which additional hepatokines might also contribute.

STAR⋆METHODS

KEY RESOURCES TABLE

REAGENT or RESOURCE	SOURCE	IDENTIFIER
Antibodies		
beta 3 Adrenergic Receptor antibody	Abcam	Cat# ab94506, RRID: AB_10863818
Anti-rabbit IgG, HRP-linked Antibody	Cell Signaling Technology	Cat# 7074, RRID: AB_2099233)
Biological samples		
Murine liver	This paper	N/A
Murine skeletal muscle	This paper	N/A
Murine brown adipose tissue	This paper	N/A
Murine white adipose tissue	This paper	N/A
Murine primary hepatocytes	This paper	N/A
Chemicals, peptides, and recombinant proteins		
50% Dextrose Injection, USP	Hospira, Inc	Provided by Boston Children’s Hospital
Humulin® R U-100	Eli Lilly And Company	Provided by Boston Children’s Hospital
Penicillin-Streptomycin (10,000 U/mL)	GIBCO	Cat# 15140122
0.9% Sodium Chloride Injection, USP	Hospira, Inc	Cat# NDC 0409-4888-20
William’s E Medium	GIBCO	Cat# 122551032
Fetal Bovine Serum	GIBCO	Cat# 16140071
DMEM - Dulbecco’s Modified Eagle Medium	GIBCO®	Cat# 12430062
Sodium pyruvate	Sigma-Aldrich	Cat# 5280
SYBR Green PCR Master Mix	Applied Biosystems	Cat# 4334973
iScript cDNA Synthesis Kit	BIO-RAD	Cat# 1708891BUN
PBS, pH 7.4	GIBCO	Cat# 10010023

REAGENT or RESOURCE	SOURCE	IDENTIFIER
GoTaq® Master Mixes	Promega Corporation	Cat# M7123
32% Paraformaldehyde aqueous solution,	Electron Microscopy Sciences	Cat# 15714S
Deoxy-D-glucose, 2-[1-14C]-, Aqueous Sol	PerkinElmer	Cat# NEC495A001MC
0.3 N Barium hydroxide solution	Sigma-Aldrich	Cat# B4059-500ML
0.3 N Zinc sulfate solution	Sigma-Aldrich	Cat# Z2876-500ML
CL 316,243 hydrate	Sigma-Aldrich	Cat# C5976
Critical commercial assays		
Mouse/Rat FGF-21 Immunoassay	R&D Systems	Cat# MF2100
Ultra-Sensitive Mouse Insulin ELISA Kit	Crystal Chem	Cat# 90080
CONTOUR® Blood Glucose Test Strips	Bayer	Cat# 7097C
Triglyceride Quantification Colorimetric/Fluorometric Kit	BioVision, Inc	Cat# K622
Experimental models: cell lines		
293A Cell Line	Invitrogen	Cat# R70507
Murine primary hepatocytes	This paper	N/A
Experimental models: organisms/strains		
Irs1/Irs2 double knockout mice (LDKO)	Provided by Dr. Morris White	N/A
Irs1/Irs2/FoxO1 triple knockout mice (LTKO)	Provided by Dr. Morris White	N/A
Albumin-Cre mice	The Jackson Laboratory	RRID: IMSR_JAX:003574
Oligonucleotides		
Primers for qPCR	Please see table in RNA isolation and real-time quantitative PCR (RT-qPCF) in STAR Methods section	N/A
shFgF21^{AdV}	This paper	N/A
scRNA^{AdV} (Ad-GFP-U6-shRNA)	VECTOR BIOLABS	Cat# 1122
FgF21^{AdV}	This paper	N/A
GFP^{AdV}	Tao et al., 2018	N/A
Foxo1^{AdV}	Addgene (Ramaswamy et al., 2002).	Cat# 9036
shFoxo1^{AdV}	Tao et al., 2018	N/A
Recombinant DNA		
pShuttle-IRES-hrGFP-2	Agilent Technologies	Cat# 240082
pAdEasy-1 vector	Agilent Technologies	Cat# 240005
pAd/BLOCK-iT, Gateway®	ThermoFisher Scientific	Cat# K494100
BLOCK-iT U6 RNAi Entry Vector Kit	ThermoFisher Scientific	Cat# K494500
Software and algorithms		
GraphPad PRISM	N/A	http://graphpad.com

REAGENT or RESOURCE	SOURCE	IDENTIFIER
BLOCK-iT siRNAs	ThermoFisher Scientific	http://rnaidesigner.thermofisher.com/rnaiexpress/
JASP	University of Amsterdam	http://jasp-stats.or/
cellSens Imaging Software	OLYMPUS CORPORATION	http://olympus-lifescience.com/
Other		
Rodent Diet With 60 kcal% Fat	Research Diets Inc.	Cat# D12492i
BAT-10 Multipurpose Thermometer	Physitemp Instruments, LLC	http://physitemp.com/
CLAMS Comprehensive Lab Animal Monitoring System: Oxymax®-CLAMS	Columbus Instruments International	Provided by the METABOLIC CORE in Brigham and Women's hospital
Dual energy X-ray absorptiometry	Lunar PIXImus, GE Lunar Corp.	Provided by the Animal Resources at Children's Hospital (ARCH)
Olympus bx43 system microscope	OLYMPUS CORPORATION	http://olympus-lifescience.com

RESOURCE AVAILABILITY

Lead contact—Further information and requests for resources and reagents should be directed to and will be fulfilled by the Lead Contact, Morris F. White (Morris.White@childrens.harvard.edu).

Materials availability—This study did not generate new unique reagents.

Data and code availability—This study did not generate/analyze datasets/code.

EXPERIMENTAL MODEL AND SUBJECT DETAILS

Animals—Liver-specific *Irs1* and *Irs2* double knockout (LDKO), and *Irs1, Irs2* and *Foxo1* triple knockout (LTKO) mice were generated as previously described (Dong et al., 2008). All pups were genotyped by PCR of genomic DNA isolated from tail-snips taken prior to 21 days of age. Control and experimental mice from the same litters were co-housed in plastic cages. All mice were fed either standard chow diet (CD) or high fat diet (HFD), maintained on a 12/12-hour light/dark cycle with free access to food and water unless otherwise indicated. Tissues of interest were removed, frozen in liquid nitrogen and stored at −80°C until RNA and protein analyses were performed. All animal experiments were performed according to procedures by the Institutional Animal Care and Use Committee at Children's Hospital Boston. Sex, age, and number of animals used in individual experiments are indicated in each figure legend.

Primary hepatocyte isolation—Primary hepatocytes were isolated from 3-month-old male wild-type mouse liver essentially as described previously (Tao et al., 2018). In brief, 12-week-old liver knockout mice and control floxed mice were anesthetized by intraperitoneal injection of Ketamin/Xylazine (120mg/kg and 10mg/kg body weight). The abdominal cavity of fully anesthetized mice was opened. After locating vena cava and portal vein a perfusion catheter was placed into vena cava. Using a peristaltic pump at 1.6 ml/min for 12 min mice were perfused with pre-warmed Hank's perfusion solution.

By an incision at the portal vein a perfusion solution outlet was generated. Following the Hank's perfusion solution, mice were perfused with pre-warmed (37°C) Liver Digest Medium (Invitrogen, 17703) at a rate of 1.6 ml/min for 12 min. Livers were dissected and immediately transferred to a Petri dish containing 10 mL L-15 medium (Invitrogen, 21083) with 10%FBS.The cells were washed three times with Hepatocyte Wash Buffer (Invitrogen, 17704) and re-suspended in William's E medium (Invitrogen, 12551) containing Percoll beads (Sigma, p4937). Primary hepatocytes were incubated in William's E medium containing 10% FBS penicillin and streptomycin for 4 hr. After 4 hr. unattached cells were removed by washing with PBS and the remaining hepatocytes were cultured in maintenance media (William's E medium containing 100μM Dex, Insulin-Transferrin-Selenium, 2mM glutamine and PenStrep) at 37°C and 5% CO_2.

METHOD DETAILS

High-fat diet feeding—Mice were fed HFD (Research Diet: R12492i) containing 60 kcal% from fat, 20 kcal% from carbohydrate and 20 kcal% from protein starting directly after weaning (day 21).

Fasting/refeeding—Mice were fasted overnight for 16 hours and then refed for 4 hours with standard regular chow diet. After 4 hours mice were sacrificed and tissues of interest were removed, frozen in liquid nitrogen, and stored at −80°C.

***In vivo* [^{14}C]2DOG (2-[1-14C]-deoxy-D-glucose) uptake assay—**Uptake of [^{14}C]2DOG into mouse tissues was performed and measured closely following the protocol previously described (Stanford et al., 2013). In brief, mice were fasted for 4 h two hours after the beginning of the light cycle. The mice were anesthetized with pentobarbital (85-100 mg/kg i.p.) and bled from the tail vein (25 μl) to assess baseline blood glucose concentration and counting of plasma ^{14}C background radiation. Mice were injected i.v. via the retro-orbital sinus, with 0.33 μCi/g body weight of [^{14}C]2DOG in combination with saline or 1 mU/g insulin. Blood samples were drawn from the tail vein at 5, 15, 30, and 45 minutes after injection for determination of plasma ^{14}C and blood glucose, to gauge insulin response. At 45 minutes, mice were sacrificed and eWAT, iWAT, BAT, and hindlimb skeletal muscles–including quadriceps, gastrocnemius, soleus, tibialis anterior and extensor digitorum longus–were snap frozen in liquid nitrogen for later extraction. Disappearance of [^{14}C]2DOG from blood plasma, and accumulation within tissues was determined using perchloric acid-soluble and $BaSO_4$/$Zn(OH)_2$-precipitation procedure and quantitated as described (Ferré et al., 1985).

Glucose, insulin, and pyruvate tolerance tests

Glucose tolerance test (GTT): After an overnight fast of 16 h (with free access to water) mice were weighed and basal glucose levels were recorded. Mice were injected intraperitoneally (i.p.) with 20% glucose in sterile 0.9% saline USP at a final dosage of 2 g/kg bodyweight. Blood glucose was monitored using a handheld glucometer at time points 0, 15, 30, 60, 90, and 120 minutes after injection.

Insulin tolerance test (ITT): Mice were fasted for 6 h (with free access to water) starting at 9 a.m. (approximately three hours after the beginning of the light cycle). Mice were weighed and basal glucose levels were recorded. Human insulin (Humulin, Eli Lilly) was diluted to a concentration of 0.1 IU/ml in sterile saline USP and a final dosage of 1.0 IU/kg bodyweight was injected i.p. Blood glucose was monitored using a handheld glucometer at time points 0, 15, 30, 60, 90, and 120 minutes after injection.

Pyruvate tolerance test (PTT): Mice were fasted for 16 hours and injected i.p. with pyruvate (2 g/kg body weight) dissolved in 0.9% sterile saline (adjusted to a physiological pH range). Blood glucose was monitored using a handheld glucometer at time points 0, 15, 30, 60, 90, and 120 minutes after injection.

RNA isolation and real-time quantitative PCR (RT-qPCR)—Tissues of interest were lysed in TRIzol (Ambion/Life Technologies) and RNA was extracted following the manufacture's guidelines. Approximately 1 μg of each RNA sample was used to synthesize cDNA by reverse transcription (iScript cDNA Synthesis Kit, BIO-RAD), which served as template for RT-qPCR reactions. RT-qPCR reactions in technical duplicate were performed and analyzed using SYBR Green Master Mix (Applied Biosystems) on a 384-well QuantStudio 6 Flex instrument (Applied Biosystems). RNA quantities were determined by the $\Delta\Delta C_t$ method using *Gapdh* (Glyceraldehyde 3-phosphate dehydrogenase) or *Tbp* (TATA-Box binding protein) as reference gene. For graphing of relative expression, the RNA quantities were normalized by the mean value in the designated control group. The sequences of the specific primers used in the real-time qRT-PCR are listed below:

Gene	Forward primer sequence (5'→3')	Reverse primer sequence (5'→3')
Tbx15	AACAGAACTGGACTTGAAGCC	GCTGCTTTTGCATGGTAGTGA
En1	GGGGATAAAAATTGCTCCAGGA	GGGCAGACAATCCATAGTAGAGG
Sfrp2	GGCCACGAGACCATGAAGG	GAAGAGCGAGCACAGGAACT
HoxC9	GATTTTCCGTCCTGTAGCTTCG	CGTAAGGGTGATAGACCACAGAC
Vdr	GTGCAGCGTAAGCGAGAGAT	GGATGGCGATAATGTGCTGTTG
Gpc4	CTCAAGTCGAAAAGTTGCTCGG	CTTCAAATGGTCACCGTTGATCT
HoxC8	CGGAGACGCCTCCAAATTCTA	TACAGTCGGGATATTGCACCA
HoxA5	CTCATTTTGCGGTCGCTATCC	ATCCATGCCATTGTAGCCGTA
Thbd	CACAGGCAGTCAATGCGTG	GAGCGCACTGTCATCAAATGT
Nr2f1	ACATCCGCATCTTTCAGGAAC	TGAATAGCACGATGGCTTTGAG
Acta1	CCCAAAGCTAACCGGGAGAAG	GACAGCACCGCCTGGATAG
Myh6	GCCCAGTACCTCCGAAAGTC	ATCAGGCACGAAGCACTCC
Mstn	AGTGGATCTAAATGAGGGCAGT	GGAGTACCTCGTGTTTTGTCTC
Myl2	AGGACGAGTGAACGTGAAAAAT	ACACGGTGAAGTTAATTGGACC
Tnni1	GCTGAGAAGGTGCGTTACCTC	AGCTCTCGGCACAAGTCCT
Tnnc1	GCGGTAGAACAGTTGACAGAG	CCAGCTCCTTGGTGCTGAT
Tnnt1	AAGGGGAGCGTGTGGATTTTG	TCCTCCTTTTTCCGCTGTTCA

Gene	Forward primer sequence (5'→3')	Reverse primer sequence (5'→3')
Myh7	ACTGTCAACACTAAGAGGGTCA	TTGGATGATTTGATCTTCCAGGG
Myh4	AGGACCAACTGAGTGAAGTGA	GGGAAAACTCGCCTGACTCTG
Tnnc2	GAGGCCAGGTCCTACCTCAG	GGTGCCCAACTCTTTAACGCT
Tnni2	GCACCTGAAGAGTGTGATGCT	TCTCCTTCTCAGATTCTCGGC
Tnnt3	GGAACGCCAGAACAGATTGG	TGGAGGACAGAGCCTTTTTCTT
Zic1	GGGACTTTCTGTTCCGCAAC	GAAGCAGCGAAGAGACTGTG
Eva1	CCTGGCAGCCTGGTCTTAT	GGAGATCCTCATCACCAAGG
Epsti1	GAGCCACATTTCGAGAGCATC	AGCAATCAGACAGGCACTTCT
Cebpb	AACTCTCTGCTTCTCCCTCTG	AAGCCCGTAGGAACATCTTT
Cox7a1	GCTCTGGTCCGGTCTTTTAGC	GTACTGGGAGGTCATTGTCGG
Cox8b	TGTGGGGATCTCAGCCATAGT	AGTGGGCTAAGACCCATCCTG
Ppara	AACATCGAGTGTCGAATATGTGG	CCGAATAGTTCGCCGAAAGAA
Pparg	GGAAGACCACTCGCATTCCTT	GTAATCAGCAACCATTGGGTCA
Cd36	TTTCTTAAACAGGTCATACATTGCT	ACTGGTTTTCTCGCCACCTC
Cpt1	GCACACCAGGCAGTAGCTTT	CAGGAGTTGATTCCAGACAGGTA
Esrra	ACCTCTGGCAGTAGCTGGAG	ATGGCGTACAGCTTCTCAGG
Acox1	CCGCCACCTTCAATCCAGAG	CAAGTTCTCGATTTCTCGACGG
Mcad	CGAACACAACACTCGAAAGC	GGGCAGTTGCTTGAAACTCT
Ucp1	CAAAAACAGAAGGATTGCCGAAA	TCTTGGACTGAGTCGTAGAGG
Ppargc1a	TATGGAGTGACATAGAGTGTGCT	CCACTTCAATCCACCCAGAAAG
Prdm16	CCACCAGCGAGGACTTCAC	GGAGGACTCTCGTAGCTCGAA
Cidea	AATGGACACCGGGTAGTAAGT	CAGCCTGTATAGGTCGAAGGT
Slc2a1	TCAGGCGGAAGCTAGGAAC	GGAGGGAAACATGCAGTCATC
Slc2a4	GTGACTGGAACACTGGTCCTA	CCAGCCACGTTGCATTGTAG
Fgf21	CTGCTGGGGGTCTACCAAG	CTGCGCCTACCACTGTTCC
Foxo1	GTGAACACCATGCCTCACAC	CACAGTCCAAGCGCTCAATA
Tbp	CTTCCTGCCACAATGTCACAG	CCTTTCTCATGCTTGCTTCTCTG
Gapdh	AGGTCGGTGTGAACGGATTTG	GGGGTCGTTGATGGCAACA

Histology and Quantification—Portions of BAT were fixed overnight in 4% phosphate buffered paraformaldehyde. Paraffin sections were generated and stained with hematoxylin and eosin (H&E) to assess tissue histology. H&E staining was performed by the Dana-Farber/Harvard Cancer Center Rodent Histopathology Core. Images were collected using an Olympus BX43 system. Cell size quantification was performed using cellSense Standard software (Olympus Life Science). For each group, tissues from at least three mice were examined, using one or more slides containing one or more sections. Approximately 20 to 30 adipocytes were measured per section to obtain average adipocyte sizes in each biological replicate. These average sizes and their standard deviations are reported in the figures.

Adenovirus preparation and injection—Adenoviruses for Foxo1 overexpression and knock down ($Foxo1^{AdV}$ and $shFoxo1^{AdV}$) were prepared as previously described(Tao et al.,

2018). To generate Fgf21 and GFP overexpression adenoviruses ($Fgf21^{AdV}$ and GFP^{AdV}), the coding sequences for mouse *Fgf21* and mammalian codon-optimized GFP were cloned into the plasmid vector pShuttle-IRES-hrGFP-2 (Agilent), then transferred to plasmid vector pAdEasy (Agilent). Gene-specific shRNA (short hairpin RNA) for Fgf21 was designed using BLOCK-iT (Life Technologies) Synthesized DNA oligonucleotides (Integrated DNA Technologies). The oligonucleotides

mFgf21-shRNA-top

5’ CACCGGGATTCAACACAGGAGAAACTTCAAGAGAGTTTCTCCTGTGTTGAATCCC, and *mFgf21-shRNA-bottom*

5’ AAAAGGGATTCAACACAGGAGAAACTCTCTTGAAGTTTCTCCTGTGTTGAATCCC

were cloned into a pENTR/U6 vector (Life Technologies). pENTR/U6 constructs were recombined with pAd/BLOCK-iT vectors. All positive clones were transfected and amplified in HEK293A cells (Life Technologies). HEK293A were cultivated in high glucose (4.5 g/L glucose) Dulbecco’s Modified Eagle’s Medium (DMEM) supplemented with 100 units/ml penicillin, 100 units/ml streptomycin, 10% FBS and maintained at 37°C and 5% CO_2 in a humidified incubator. Adenoviruses were purified using a cesium chloride gradient ultracentrifugation and tittered using an end-point dilution method. Infection of the mouse liver with adenoviruses was accomplished by i.v. injection into the retroorbital sinus of 1.0 $x10^8$ particles of adenovirus per gram of body weight in 100 µl saline (0.9% NaCl).

Adenovirus infection in primary hepatocytes—Primary hepatocytes were isolated from 3-month-old wild-type mouse liver essentially as described previously (Tao et al., 2018) and infected 4 hours after plating by addition of adenoviruses in fresh Williams E medium (WE) containing 10% FBS and penicillin/streptomycin. After 48 hours, the medium was replaced with WE containing 1% FBS and penicillin/streptomycin for 24 hours before the hepatocytes were collected into Trizol to isolate RNA.

Blood chemistry and hormone assays—Blood used for analysis of hormones was collected after a 16 h overnight fast. Serum concentrations FGF21 and insulin were determined by ELISA assay using commercial kits (FGF21: R&D Systems, cat#MF2100; insulin: Chrystal Chem, cat#90080) according to the manufacturers’ instructions. Glucose was measured using CONTOUR blood glucose test strips and CONTOUR blood glucose meters (Bayer).

Quantification of hepatic triglycerides—Livers of mice were homogenized according to the manufacturer’s instructions (Triglyceride Quantification Colorimetric/Fluorometric Kit, Biovision, Inc, cat#K622-100). The levels of triglycerides were determined following the guidelines of Triglyceride Assay Protocol provided by the manufacturer.

Dual-energy X-ray absorptiometry (DEXA)—For analysis of fat and lean body mass, animals were anesthetized with isoflurane, using a precision vaporizer. To induce anesthesia

mice were placed into a plastic box which was flooded with oxygen and isoflurane; for maintenance of anesthesia, isoflurane was infused at a constant flow rate. Fully anesthetized mice were placed in a dual energy X-ray absorptiometer (DEXA, Lunar, PIXImus, Fitchburg, WI) and switched to a nose cone to continue anesthesia throughout data collection. At the start of each session of data collection the energy X-ray absorptiometer machine was normalized to a "phantom-mouse" provided by the manufacturer.

Measurement of acute cold tolerance

Twelve-hour cold exposure: To assess thermotolerance of CTRL and LDKO mice during 12-hour cold challenge, we used the Columbus Instruments Comprehensive Lab Animal Monitoring System (CLAMS) placed in a temperature-controlled room. For the experiment, mice were transferred to individual CLAMS metabolic cages, housed on a 12/12-hour light/dark cycle, and monitored by implantable temperature sensors (Bio Medic Data Systems, Inc.). Beginning 5.5 days before cold challenge, mice were held at thermoneutrality (22°C) for approximately 2.5 days, then at 22°C for approximately 3 days for acclimatization before cold challenge. During the 12-hour cold challenge, the ambient temperature was reduced from 22°C to 4°C during first two hours, then held at 4°C for a further 10 hours.

Two-hour cold exposure: Empty cages containing bedding, food and water were placed in a cold room (set to 4°C) overnight, allowing the cages to cool down. The next morning experimental mice were placed into these pre-chilled cages inside the cold room with free access to food and water. The baseline core temperature of each mouse was taken immediately before the mice were transferred into the cages inside the cold room. The body core temperature was monitored using a rectal probe (BAT-10 Multipurpose Thermometer, Physitemp Instruments). Each mouse was individually housed to avoid huddling. Mice were monitored, and body core temperature was measured every 30 minutes. For γ3-adrenoreceptor agonism, mice were injected i.p. with CL316,243 (1 mg/kg or 2 mg/kg) or 1x PBS (vehicle control) 1 h prior to the cold challenge.

Immunoblotting—Brown adipose tissues were lysed using a tissue homogenizer and tissue lysis buffer (50 mM HEPES, pH 7.5, 150 mM NaCl, 10% glycerol, 1% Triton X-100,1.5 mM $MgCl_2$, 1 mM EGTA, 10 mM sodium pyrophosphate, 100 mM sodium fluoride, and freshly added protease inhibitor cocktail and phosphatase inhibitor cocktail). The lysates were centrifuged, and the protein concentration of the supernatants was quantified by BCA assay (Thermo). Equalized protein extracts were applied and resolved on an SDS-PAGE, transferred to nitrocellulose membrane (BIO-RAD) and incubated with a beta 3 adrenergic receptor primary antibody (Abcam) overnight. For antibody/protein detection membranes were incubated with an anti-rabbit IgG HRP-linked secondary antibody (Cell Signaling Technology) followed by application of ECL detection reagents.

QUANTIFICATION AND STATISTICAL ANALYSIS

Statistical analyses are summarized in the figure legends. In most cases, differences between group means were assessed in Prism (GraphPad; v 8.4.3) by either unpaired Student t test or by one-way ANOVA followed by Tukey's HSD (honest significant difference) comparison of each group to every other. In cases where means were compared to a single control

mean, p values were instead corrected for multiple comparison by the Dunnett method. Factorial ANOVA of 2 × 3 or 3 × 2 data was performed using JASP (U. of Amsterdam, https://jasp-stats.org; version 0.12.2) with Type II sum of squares followed by Tukey's HSD comparison of each group to every other. All significant differences are shown in the figures.

Supplementary Material

Refer to Web version on PubMed Central for supplementary material.

ACKNOWLEDGMENTS

This work was supported by National Institutes of Health grants DK098655 and R01AG06791 to M.F.W. We thank Dr. R. DePinho for providing floxed Foxo1 mice and Dr. Alexander S. Banks (Metabolic Core, Beth Israel Deaconess Hospital, Boston, MA) for help with performance and analysis of chronic cold exposure.

REFERENCES

Adams AC, Yang C, Coskun T, Cheng CC, Gimeno RE, Luo Y, and Kharitonenkov A (2012). The breadth of FGF21's metabolic actions are governed by FGFR1 in adipose tissue. Mol. Metab 2, 31–37. [PubMed: 24024127]

Ameka M, Markan KR, Morgan DA, BonDurant LD, Idiga SO, Naber MC, Zhu Z, Zingman LV, Grobe JL, Rahmouni K, and Potthoff MJ (2019). Liver derived FGF21 maintains core body temperature during acute cold exposure. Sci. Rep 9, 630. [PubMed: 30679672]

Assini JM, Mulvihill EE, Burke AC, Sutherland BG, Telford DE, Chhoker SS, Sawyez CG, Drangova M, Adams AC, Kharitonenkov A, et al. (2015). Naringenin prevents obesity, hepatic steatosis, and glucose intolerance in male mice independent of fibroblast growth factor 21. Endocrinology 156, 2087–2102. [PubMed: 25774553]

Badman MK, Pissios P, Kennedy AR, Koukos G, Flier JS, and Maratos-Flier E (2007). Hepatic fibroblast growth factor 21 is regulated by PPARalpha and is a key mediator of hepatic lipid metabolism in ketotic states. Cell Metab. 5, 426–437. [PubMed: 17550778]

Badman MK, Koester A, Flier JS, Kharitonenkov A, and Maratos-Flier E (2009). Fibroblast growth factor 21-deficient mice demonstrate impaired adaptation to ketosis. Endocrinology 150, 4931–4940. [PubMed: 19819944]

Beenken A, and Mohammadi M (2009). The FGF family: biology, pathophysiology and therapy. Nat. Rev. Drug Discov 8, 235–253. [PubMed: 19247306]

BonDurant LD, and Potthoff MJ (2018). Fibroblast growth factor 21: a versatile regulator of metabolic homeostasis. Annu. Rev. Nutr 38, 173–196. [PubMed: 29727594]

BonDurant LD, Ameka M, Naber MC, Markan KR, Idiga SO, Acevedo MR, Walsh SA, Ornitz DM, and Potthoff MJ (2017). FGF21 regulates metabolism through adipose-dependent and -independent mechanisms. Cell Metab. 25, 935–944.e4. [PubMed: 28380381]

Camporez JP, Jornayvaz FR, Petersen MC, Pesta D, Guigni BA, Serr J, Zhang D, Kahn M, Samuel VT, Jurczak MJ, and Shulman GI (2013). Cellular mechanisms by which FGF21 improves insulin sensitivity in male mice. Endocrinology 154, 3099–3109. [PubMed: 23766126]

Camporez JP, Asrih M, Zhang D, Kahn M, Samuel VT, Jurczak MJ, and Jornayvaz FR (2015). Hepatic insulin resistance and increased hepatic glucose production in mice lacking Fgf21. J. Endocrinol 226, 207–217. [PubMed: 26203166]

Cannon B, and Nedergaard J (2004). Brown adipose tissue: function and physiological significance. Physiol. Rev 84, 277–359. [PubMed: 14715917]

Cannon B, and Nedergaard J (2011). Nonshivering thermogenesis and its adequate measurement in metabolic studies. J. Exp. Biol 214, 242–253. [PubMed: 21177944]

Chartoumpekis DV, Habeos IG, Ziros PG, Psyrogiannis AI, Kyriazopoulou VE, and Papavassiliou AG (2011). Brown adipose tissue responds to cold and adrenergic stimulation by induction of FGF21. Mol. Med 17, 736–740. [PubMed: 21373720]

Cheng Z, Guo S, Copps K, Dong X, Kollipara R, Rodgers JT, Depinho RA, Puigserver P, and White MF (2009). Foxo1 integrates insulin signaling with mitochondrial function in the liver. Nat. Med 15, 1307–1311. [PubMed: 19838201]

Chondronikola M, Volpi E, Børsheim E, Porter C, Annamalai P, Enerbäck S, Lidell ME, Saraf MK, Labbe SM, Hurren NM, et al. (2014). Brown adipose tissue improves whole-body glucose homeostasis and insulin sensitivity in humans. Diabetes 63, 4089–4099. [PubMed: 25056438]

Czech MP (2017). Insulin action and resistance in obesity and type 2 diabetes. Nat. Med 23, 804–814. [PubMed: 28697184]

Dong XC, Copps KD, Guo S, Li Y, Kollipara R, DePinho RA, and White MF (2008). Inactivation of hepatic Foxo1 by insulin signaling is required for adaptive nutrient homeostasis and endocrine growth regulation. Cell Metab. 8, 65–76. [PubMed: 18590693]

El Ouaamari A, O-Sullivan I, Shirakawa J, Basile G, Zhang W, Roger S, Thomou T, Xu S, Qiang G, Liew CW, et al. (2019). Forkhead box protein O1 (FoxO1) regulates hepatic serine protease inhibitor B1 (serpinB1) expression in a non-cell-autonomous fashion. J. Biol. Chem 294, 1059–1069. [PubMed: 30459233]

Emanuelli B, Vienberg SG, Smyth G, Cheng C, Stanford KI, Arumugam M, Michael MD, Adams AC, Kharitonenkov A, and Kahn CR (2014). Interplay between FGF21 and insulin action in the liver regulates metabolism. J. Clin. Invest 124, 515–527. [PubMed: 24401271]

Ferré P, Leturque A, Burnol AF, Penicaud L, and Girard J (1985). A method to quantify glucose utilization in vivo in skeletal muscle and white adipose tissue of the anaesthetized rat. Biochem. J 228, 103–110. [PubMed: 3890836]

Fisher SJ, and Kahn CR (2003). Insulin signaling is required for insulin's direct and indirect action on hepatic glucose production. J. Clin. Invest 111, 463–468. [PubMed: 12588884]

Fisher FM, and Maratos-Flier E (2016). Understanding the physiology of FGF21. Annu. Rev. Physiol 78, 223–241. [PubMed: 26654352]

Fisher FM, Kleiner S, Douris N, Fox EC, Mepani RJ, Verdeguer F, Wu J, Kharitonenkov A, Flier JS, Maratos-Flier E, and Spiegelman BM (2012). FGF21 regulates PGC-1α and browning of white adipose tissues in adaptive thermogenesis. Genes Dev. 26, 271–281. [PubMed: 22302939]

Guo S, Copps KD, Dong X, Park S, Cheng Z, Pocai A, Rossetti L, Sajan M, Farese RV, and White MF (2009). The Irs1 branch of the insulin signaling cascade plays a dominant role in hepatic nutrient homeostasis. Mol. Cell. Biol 29, 5070–5083. [PubMed: 19596788]

Haas JT, Miao J, Chanda D, Wang Y, Zhao E, Haas ME, Hirschey M, Vaitheesvaran B, Farese RV Jr., Kurland IJ, et al. (2012). Hepatic insulin signaling is required for obesity-dependent expression of SREBP-1c mRNA but not for feeding-dependent expression. Cell Metab. 15, 873–884. [PubMed: 22682225]

Haeusler RA, Han S, and Accili D (2010). Hepatic FoxO1 ablation exacerbates lipid abnormalities during hyperglycemia. J. Biol. Chem 285, 26861–26868. [PubMed: 20573950]

Hansen JS, Clemmesen JO, Secher NH, Hoene M, Drescher A, Weigert C, Pedersen BK, and Plomgaard P (2015). Glucagon-to-insulin ratio is pivotal for splanchnic regulation of FGF-21 in humans. Mol. Metab 4, 551–560. [PubMed: 26266087]

Harms MJ, Ishibashi J, Wang W, Lim HW, Goyama S, Sato T, Kurokawa M, Won KJ, and Seale P (2014). Prdm16 is required for the maintenance of brown adipocyte identity and function in adult mice. Cell Metab. 19, 593–604. [PubMed: 24703692]

Hondares E, Rosell M, Gonzalez FJ, Giralt M, Iglesias R, and Villarroya F (2010). Hepatic FGF21 expression is induced at birth via PPARalpha in response to milk intake and contributes to thermogenic activation of neonatal brown fat. Cell Metab. 11, 206–212. [PubMed: 20197053]

Hotta Y, Nakamura H, Konishi M, Murata Y, Takagi H, Matsumura S, Inoue K, Fushiki T, and Itoh N (2009). Fibroblast growth factor 21 regulates lipolysis in white adipose tissue but is not required for ketogenesis and triglyceride clearance in liver. Endocrinology 150, 4625–4633. [PubMed: 19589869]

Ido-Kitamura Y, Sasaki T, Kobayashi M, Kim HJ, Lee YS, Kikuchi O, Yokota-Hashimoto H, Iizuka K, Accili D, and Kitamura T (2012). Hepatic FoxO1 integrates glucose utilization and lipid synthesis through regulation of Chrebp O-glycosylation. PLoS ONE 7, e47231. [PubMed: 23056614]

Inagaki T, Dutchak P, Zhao G, Ding X, Gautron L, Parameswara V, Li Y, Goetz R, Mohammadi M, Esser V, et al. (2007). Endocrine regulation of the fasting response by PPARalpha-mediated induction of fibroblast growth factor 21. Cell Metab. 5,415–425. [PubMed: 17550777]

Kharitonenkov A, Shiyanova TL, Koester A, Ford AM, Micanovic R, Galbreath EJ, Sandusky GE, Hammond LJ, Moyers JS, Owens RA, et al. (2005). FGF-21 as a novel metabolic regulator. J. Clin. Invest 115, 1627–1635. [PubMed: 15902306]

Kliewer SA, and Mangelsdorf DJ (2019). A dozen years of discovery: insights into the physiology and pharmacology of FGF21. Cell Metab. 29, 246–253. [PubMed: 30726758]

Kuro-o M (2018). Ageing-related receptors resolved. Nature 553, 409–410.

Li Q, Zhang Y, Ding D, Yang Y, Chen Q, Su D, Chen X, Yang W, Qiu J, and Ling W (2016). Association between serum fibroblast growth factor 21 and mortality among patients with coronary artery disease. J. Clin. Endocrinol. Metab 101, 4886–4894. [PubMed: 27662438]

Ling AV, Gearing ME, Semova I, Shin DJ, Clements R, Lai ZW, and Biddinger SB (2018). FoxO1 is required for most of the metabolic and hormonal perturbations produced by hepatic insulin receptor deletion in male mice. Endocrinology 159, 1253–1263. [PubMed: 29300910]

Liu J, DeYoung SM, Hwang JB, O'Leary EE, and Saltiel AR (2003).The roles of Cbl-b and c-Cbl in insulin-stimulated glucosetransport. J. Biol. Chem 278, 36754–36762. [PubMed: 12842890]

Liu T, Yu B, Kakino M, Fujimoto H, Ando Y, Hakuno F, and Takahashi SI (2016). A novel IRS-1-associated protein, DGKζ regulates GLUT4 translocation in 3T3-L1 adipocytes. Sci. Rep 6, 35438. [PubMed: 27739494]

Lu M, Wan M, Leavens KF, Chu Q, Monks BR, Fernandez S, Ahima RS, Ueki K, Kahn CR, and Birnbaum MJ (2012). Insulin regulates liver metabolism in vivo in the absence of hepatic Akt and Foxo1. Nat. Med 18, 388–395. [PubMed: 22344295]

Markan KR, Naber MC, Ameka MK, Anderegg MD, Mangelsdorf DJ, Kliewer SA, Mohammadi M, and Potthoff MJ (2014). Circulating FGF21 is liver derived and enhances glucose uptake during refeeding and overfeeding. Diabetes 63, 4057–4063. [PubMed: 25008183]

Mashili FL, Austin RL, Deshmukh AS, Fritz T, Caidahl K, Bergdahl K, Zierath JR, Chibalin AV, Moller DE, Kharitonenkov A, and Krook A (2011). Direct effects of FGF21 on glucose uptake in human skeletal muscle: implications for type 2 diabetes and obesity. Diabetes Metab. Res. Rev 27, 286–297. [PubMed: 21309058]

Matsumoto M, Han S, Kitamura T, and Accili D (2006). Dual role of transcription factor FoxO1 in controlling hepatic insulin sensitivity and lipid metabolism. J. Clin. Invest 116, 2464–2472. [PubMed: 16906224]

Meex RCR, and Watt MJ (2017). Hepatokines: linking nonalcoholic fatty liver disease and insulin resistance. Nat. Rev. Endocrinol 13, 509–520. [PubMed: 28621339]

Michos ED, Vaidya D, Gapstur SM, Schreiner PJ, Golden SH, Wong ND, Criqui MH, and Ouyang P (2008). Sex hormones, sex hormone binding globulin, and abdominal aortic calcification in women and men in the multiethnic study of atherosclerosis (MESA). Atherosclerosis 200, 432–438. [PubMed: 18262187]

Nedergaard J, Golozoubova V, Matthias A, Asadi A, Jacobsson A, and Cannon B (2001). UCP1: the only protein able to mediate adaptive non-shivering thermogenesis and metabolic inefficiency. Biochim. Biophys. Acta 1504, 82–106. [PubMed: 11239487]

O-Sullivan I, Zhang W, Wasserman DH, Liew CW, Liu J, Paik J, De-Pinho RA, Stolz DB, Kahn CR, Schwartz MW, and Unterman TG (2015). FoxO1 integrates direct and indirect effects of insulin on hepatic glucose production and glucose utilization. Nat. Commun 6, 7079. [PubMed: 25963540]

Peres Valgas C. da Silva., Hernández-Saavedra D, White JD, and Stanford KI (2019). Cold and exercise: therapeutic tools to activate brown adipose tissue and combat obesity. Biology (Basel) 8, 9.

Perry RJ, Camporez JG, Kursawe R, Titchenell PM, Zhang D, Perry CJ, Jurczak MJ, Abudukadier A, Han MS, Zhang XM, et al. (2015). Hepatic acetyl CoA links adipose tissue inflammation to hepatic insulin resistance and type 2 diabetes. Cell 160, 745–758. [PubMed: 25662011]

Petersen MC, and Shulman GI (2018). Mechanisms ofinsulin action and insulin resistance. Physiol. Rev 98, 2133–2223. [PubMed: 30067154]

Potthoff MJ, Inagaki T, Satapati S, Ding X, He T, Goetz R, Mohammadi M, Finck BN, Mangelsdorf DJ, Kliewer SA, and Burgess SC (2009). FGF21 induces PGC-1alpha and regulates carbohydrate and fatty acid metabolism during the adaptive starvation response. Proc. Natl. Acad. Sci. USA 106, 10853–10858. [PubMed: 19541642]

Ramaswamy S, Nakamura N, Sansal I, Bergeron L, and Sellers WR (2002). A novel mechanism of gene regulation and tumor suppression by the transcription factor FKHR. Cancer Cell 2, 81–91. [PubMed: 12150827]

Roden M, and Shulman GI (2019). The integrative biology of type 2 diabetes. Nature 576, 51–60. [PubMed: 31802013]

Rosen ED, and Spiegelman BM (2006). Adipocytes as regulators ofenergy balance and glucose homeostasis. Nature 444, 847–853. [PubMed: 17167472]

Schoettl T, Fischer IP, and Ussar S (2018). Heterogeneity of adipose tissue in development and metabolic function. J. Exp. Biol 221, jeb162958.

Seale P, Bjork B, Yang W, Kajimura S, Chin S, Kuang S, Scime A, Devarakonda S, Conroe HM, Erdjument-Bromage H, et al. (2008). PRDM16 controls a brown fat/skeletal muscle switch. Nature 454, 961–967. [PubMed: 18719582]

Shin DJ, Joshi P, Hong SH, Mosure K, Shin DG, and Osborne TF (2012). Genome-wide analysis of FoxO1 binding in hepatic chromatin: potential involvement of FoxO1 in linking retinoid signaling to hepatic gluconeogenesis. Nucleic Acids Res. 40, 11499–11509. [PubMed: 23066095]

Staiger H, Keuper M, Berti L, Hrabe de Angelis M, and Haring HU (2017). Fibroblast growth factor 21-metabolic role in mice and men. Endocr. Rev 38, 468–488. [PubMed: 28938407]

Stanford KI, Middelbeek RJ, Townsend KL, An D, Nygaard EB, Hitchcox KM, Markan KR, Nakano K, Hirshman MF, Tseng YH, and Goodyear LJ (2013). Brown adipose tissue regulates glucose homeostasis and insulin sensitivity. J. Clin. Invest 123, 215–223. [PubMed: 23221344]

Stefan N, and Haring HU (2013). The role of hepatokines in metabolism. Nat. Rev. Endocrinol 9, 144–152. [PubMed: 23337953]

Tan SX, Fisher-Wellman KH, Fazakerley DJ, Ng Y, Pant H, Li J, Meoli CC, Coster AC, Stöckli J, and James DE (2015). Selective insulin resistance in adipocytes. J. Biol. Chem 290, 11337–11348. [PubMed: 25720492]

Tao R, Wang C, Stöhr O, Qiu W, Hu Y, Miao J, Dong XC, Leng S, Stefater M, Stylopoulos N, et al. (2018). Inactivating hepatic follistatin alleviates hyperglycemia. Nat. Med 24, 1058–1069. [PubMed: 29867232]

Titchenell PM, Quinn WJ, Lu M, Chu Q, Lu W, Li C, Chen H, Monks BR, Chen J, Rabinowitz JD, and Birnbaum MJ (2016). Direct hepatocyte insulin signaling is required for lipogenesis but is dispensable forthe suppression of glucose production. Cell Metab. 23, 1154–1166. [PubMed: 27238637]

Townsend KL, and Tseng YH (2014). Brown fat fuel utilization and thermogenesis. Trends Endocrinol. Metab 25, 168–177. [PubMed: 24389130]

Xu J, Lloyd DJ, Hale C, Stanislaus S, Chen M, Sivits G, Vonderfecht S, Hecht R, Li YS, Lindberg RA, et al. (2009a). Fibroblast growth factor 21 reverses hepatic steatosis, increases energy expenditure, and improves insulin sensitivity in diet-induced obese mice. Diabetes 58, 250–259. [PubMed: 18840786]

Xu J, Stanislaus S, Chinookoswong N, Lau YY, Hager T, Patel J, Ge H, Weiszmann J, Lu SC, Graham M, et al. (2009b). Acute glucose lowering and insulin-sensitizing action of FGF21 in insulin-resistant mouse models–association with liver and adipose tissue effects. Am. J. Physiol. Endocrinol. Metab 297, E1105–E1114. [PubMed: 19706786]

Yang SJ, Hwang SY, Choi HY, Yoo HJ, Seo JA, Kim SG, Kim NH, Baik SH, Choi DS, and Choi KM (2011). Serum selenoprotein P levels in patients with type 2 diabetes and prediabetes: implications for insulin resistance, inflammation, and atherosclerosis. J. Clin. Endocrinol. Metab 96, E1325–E1329. [PubMed: 21677040]

Yang C, Jin C, Li X, Wang F, McKeehan WL, and Luo Y (2012). Differential specificity of endocrine FGF19 and FGF21 to FGFR1 and FGFR4 in complex with KLB. PLoS ONE 7, e33870. [PubMed: 22442730]

Yoshida T, Umekawa T, Sakane N, Yoshimoto K, and Kondo M (1996). Effect of CL316,243, a highly specific beta3-adrenoceptor agonist, on sympathetic nervous system activity in mice. Metabolism 45, 787–791. [PubMed: 8637456]

Zhao LP, Xu WT, Wang L, You T, Chan SP, Zhao X, and Yang XJ (2015). Serum adropin level in patients with stable coronary artery disease. Heart Lung Circ. 24, 975–979. [PubMed: 25912996]

Highlights

- "LDKO" mice lacking hepatic Irs1 and Irs2 model severe hepatic insulin resistance
- Hepatic FoxO1 in LDKO mice suppresses Fgf21 in a cell-autonomous fashion
- Lower Fgf21 impairs brown adipose tissue (BAT) gene expression and thermogenesis
- Hepatic Foxo1 deletion or adenoviral Fgf21 restores BAT function in LDKO mice

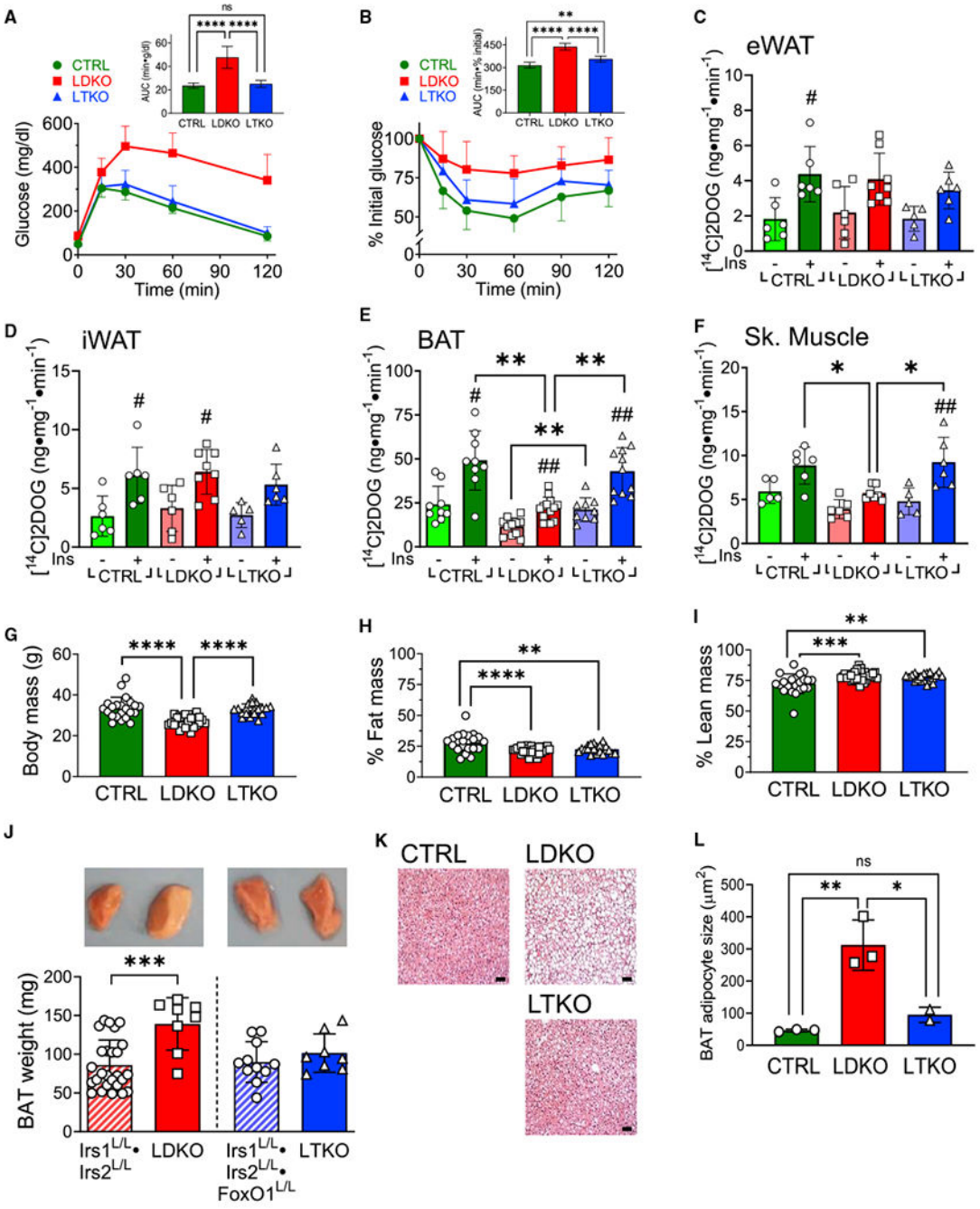

Figure 1. Hepatic FoxO1 in LDKO mice dysregulates BAT and muscle glucose utilization and promotes lipid accumulation in brown adipocytes

(A and B) Glucose homeostasis in 12- to 13-week-old male mice assessed by (A) glucose tolerance test (n = 7, 8, and 12 mice) and (B) insulin tolerance test (n = 8, 6, and 8 mice). Inset graphs show areas under curves (AUCs).

(C–F) Basal and insulin-stimulated uptake of [^{14}C]2DOG into (C) epigonadal WAT, (D) inguinal WAT, (E) interscapular BAT, or (F) combined hindlimb skeletal muscles (Sk. muscle) of 14-week-old male mice (n = 5–8 mice for eWAT, iWAT, and Sk. muscle; n = 9–13 mice for BAT).

(G–I) Body weights and body composition of 24-week-old CTRL, LDKO, and LTKO male mice (n = 22, 30, and 20 mice). DEXA-determined (H) fat mass and (I) lean masses are expressed as percentages of body weights in (G).

(J) Weights of dissected interscapular BAT in 14- to 16-week-old male mice and respective double-floxed ($Irs1^{L/L}$·$Irs2^{L/L}$) or triple-floxed ($Irs1^{L/L}$·$Irs2^{L/L}$·$FoxO1^{L/L}$) controls. Pictures show representative BAT depots.(K) Representative H&E-stained BAT sections (“CTRL” = $Irs1^{L/L}$·$Irs2^{L/L}$). Scale bar, 50 μm.

(L) Quantification of adipocyte sizes in H&E-stained BAT sections. Points represent average area of individual adipocytes (n ≈ 20–30) in BAT samples from unique mice (n = 3, 3, and 2 mice).

Lines or bars and error bars represent mean values ± SD. Differences between means were assessed by one-way ANOVA (A, B, G–J, and L) or by 2 × 3 factorial ANOVA (C–F), followed by Tukey’s HSD (honest significant difference)-based comparison of each group to every other: *p < 0.05; **p < 0.01; ***p < 0.001; ****p < 0.0001; ns, not significant. In (C)–(F), #p < 0.05 and ##p < 0.01 versus same genotype not treated with insulin.

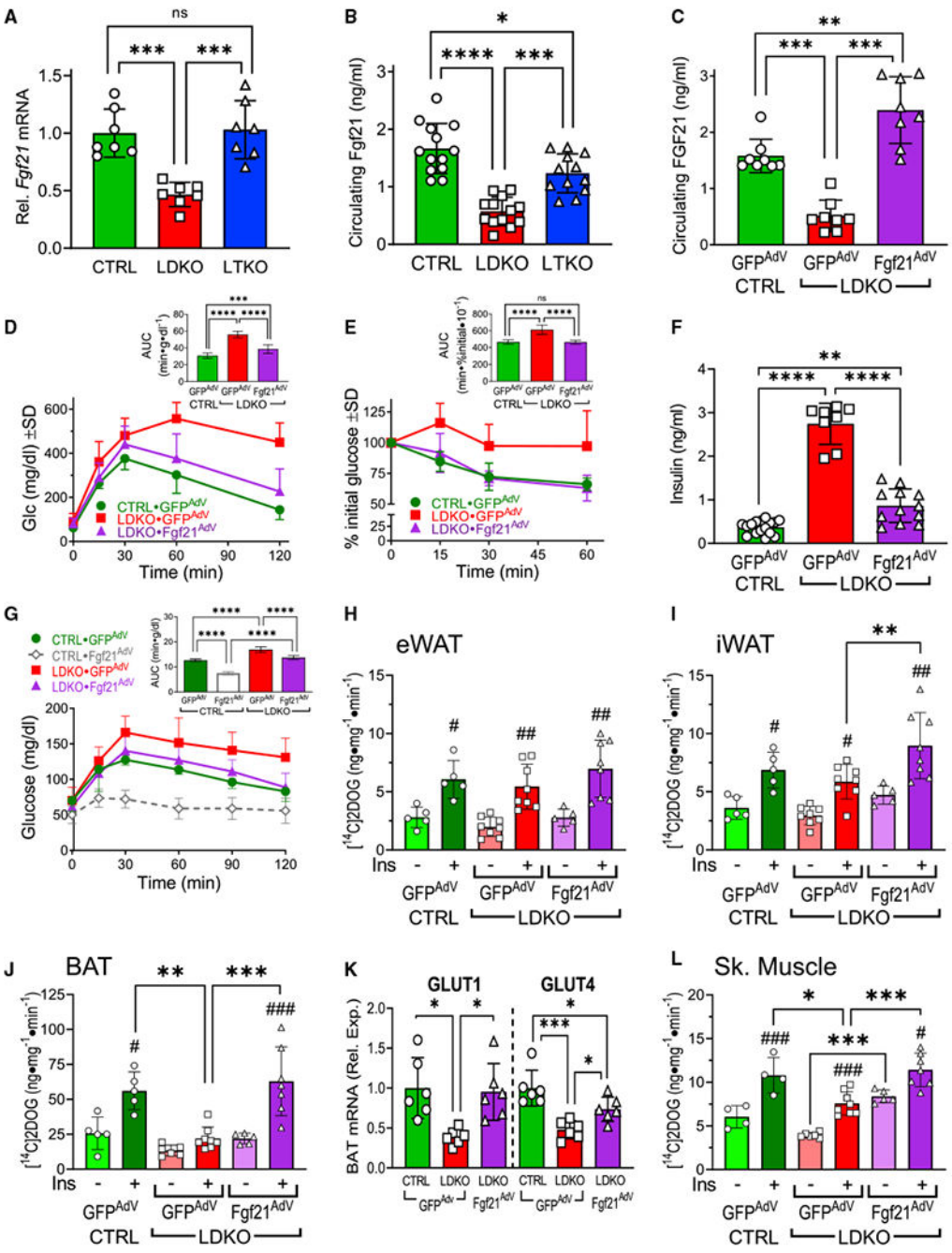

Figure 2. Correction of hepatic Fgf21 insufficiency in LDKO mice normalizes BAT and muscle glucose uptake and restores peripheral insulin sensitivity

(A) *Fgf21* mRNA expression in liver of fasted 16-week-old male mice (n = 7 mice per group). Data are normalized by the CTRL mean.

(B) Serum Fgf21 concentration in fasted 12-week-old male mice (n = 13, 13, and 12 mice).

(C) Serum Fgf21 concentration in fasted male mice 12 days after infection of the liver with GFP^{AdV} or $Fgf21^{AdV}$ (n = 8 mice per group).

(D and E) Glucose homeostasis 12–19 days after infection of mice with GFP^{AdV} or $Fgf21^{AdV}$, assessed by (D) glucose tolerance (n = 10, 16, and 16 mice) and (E) insulin tolerance tests (n = 13, 6, and 6 mice). Inset shows AUCs.

(F) Serum insulin concentration 12 days after infection with GFP^{AdV} or $Fgf21^{AdV}$ (n = 16, 8, and 10 mice).

(G) Pyruvate tolerance test of HGP, approximately 24 days after infection with GFP^{AdV} or $Fgf21^{AdV}$ (n = 6, 7, 7, and 7 mice). Inset shows AUCs.

(H–J) Basal and insulin-stimulated uptake of [^{14}C]2DOG into (H) epigonadal WAT, (I) inguinal WAT, or (J) interscapular BAT 12 days after infection of mice with GFP^{AdV} or $Fgf21^{AdV}$ (n = 5 and 5 CTRL·GFP^{AdV}, 8 and 7 LDKO·GFP^{AdV}, and 5 and 8 LDKO·$Fgf21^{AdV}$ mice).

(K) Expression of GLUT1 (*Slc2a1*) and GLUT4 (*Slc2a4*) mRNAs in CTRL and LDKO BAT, 12 days after infection with GFP^{AdV} or $Fgf21^{AdV}$ (n = 6 mice per group). RNA quantities are expressed relative to CTRL means.

(L) Basal and insulin-stimulated uptake of [^{14}C]2DOG into combined hindlimb skeletal muscles of CTRL and LDKO male mice 12 days after infection with GFP^{AdV} or $Fgf21^{AdV}$ (n = 4 and 4 CTRL·GFP^{AdV}, 5 and 8 LDKO·GFP^{AdV}, and 5 and 7 LDKO·$Fgf21^{AdV}$ mice). Lines or bars and error bars represent mean values ± SD. Differences between means were assessed by unpaired t test (A), one-way ANOVA (B–G and K), or 2 × 3 factorial ANOVA (H–J and L), followed by Tukey's HSD-based comparison of each group to every other: *p < 0.05; **p < 0.01; ***p < 0.001; ****p < 0.0001 between indicated groups. In (H)–(J) and (L), #p < 0.05, ##p < 0.01, and ###p < 0.001 versus same genotype, no insulin.

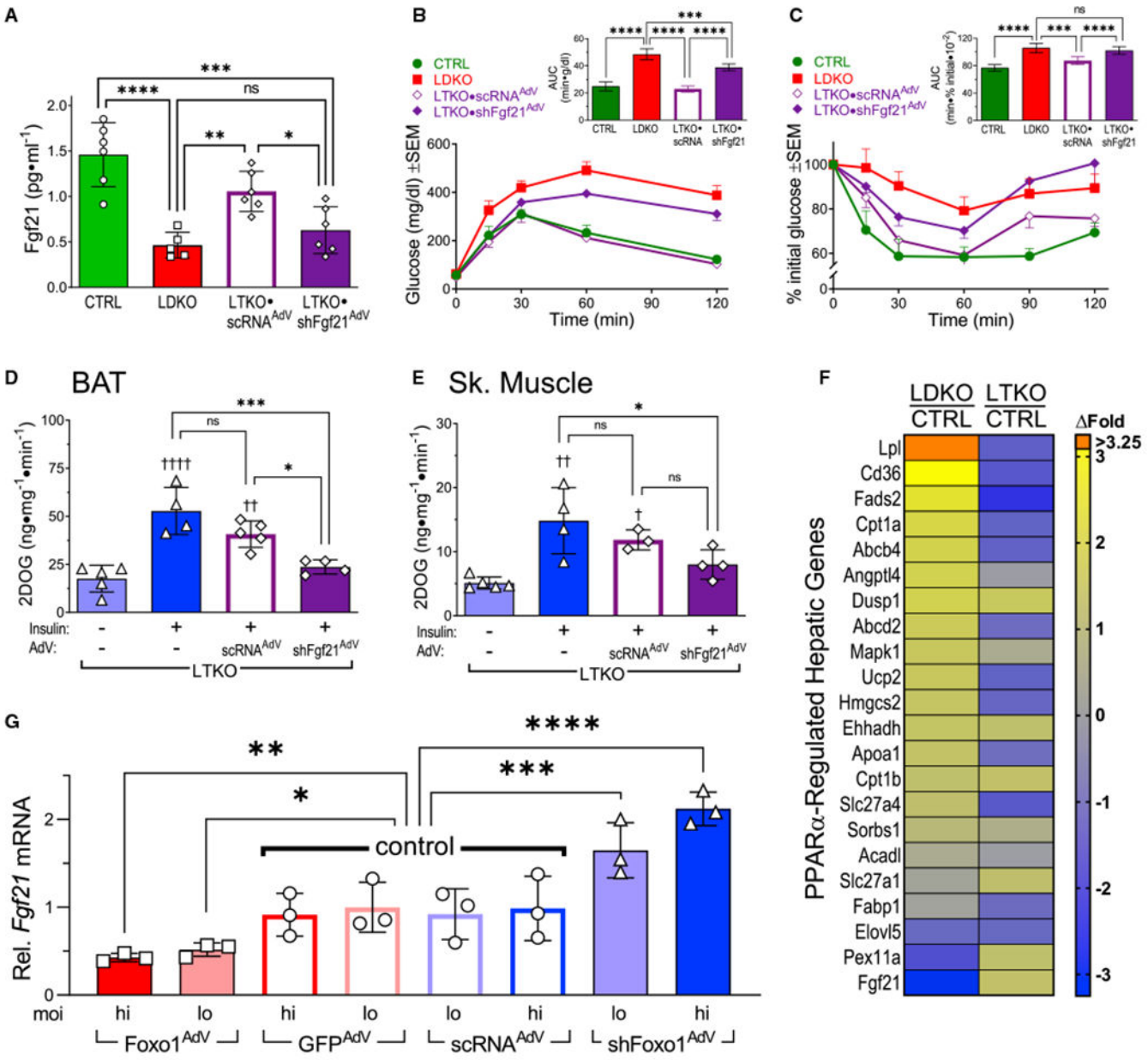

Figure 3. Normalized Fgf21 expression maintains glucose homeostasis in LTKO mice

(A) Serum Fgf21 concentration in 12-week-old male non-infected CTRL and LDKO mice or LTKO mice 12 days after infection with $scRNA^{AdV}$ (non-targeting control virus) or $shFgf21^{AdV}$ (n = 6, 5, 6, and 6 mice).

(B and C) Glucose homeostasis in control and adenovirus-infected mice, assessed by (B) glucose tolerance (n = 7, 5, 7, and 6 mice) and (C) insulin tolerancetests (n = 5, 7, 6, and 6 mice) performed 10 or 17 days after infection, respectively. Inset graphs show AUCs.

(D and E) Basal or insulin-stimulated uptake of [^{14}C]2DOG into (D) BAT or (E) skeletal muscle of non-infected LTKO mice and LTKO mice infected with $scRNA^{AdV}$ or $shFgf21^{AdV}$ (BAT: n = 5, 4, 5, and 4 mice; Sk. muscle: n = 5, 4, 3, and 4 mice). Glucose uptake was assessed approximately 3.5 weeks after infection.

(F) Relative mRNA expression of known PPARα target genes in liver of fasted LDKO and LTKO mice. Color scale shows $\log_2$ fold change versus floxed CTRL liver.
(G) Expression of *Fgf21* mRNA in primary hepatocytes infected at high (600) or low (200) MOI with Foxo1^{AdV} to overexpress *Foxo1* or with shFoxo1^{AdV} to knock down *Foxo1* expression. All data are expressed relative to the *Fgf21* mRNA level in hepatocytes infected with control GFP^{AdV} at low MOI.
Except for GTT and ITT curves in (B) and (C) (mean ± SEM), lines or bars and error bars represent mean values ± SD. Differences between means were assessed by one-way ANOVA, followed by (A–E) Tukey's HSD-based comparison of each group to every other or (G) comparison of each group to the average of the four control groups(open bars): *$p < 0.05$; **$p < 0.01$; ***$p < 0.001$; ****$p < 0.0001$ between indicated groups. In (D) and (E), †$p < 0.05$, ††$p < 0.01$, and †††$p < 0.001$ versus left bar (non-infected LTKO mice in basal condition).

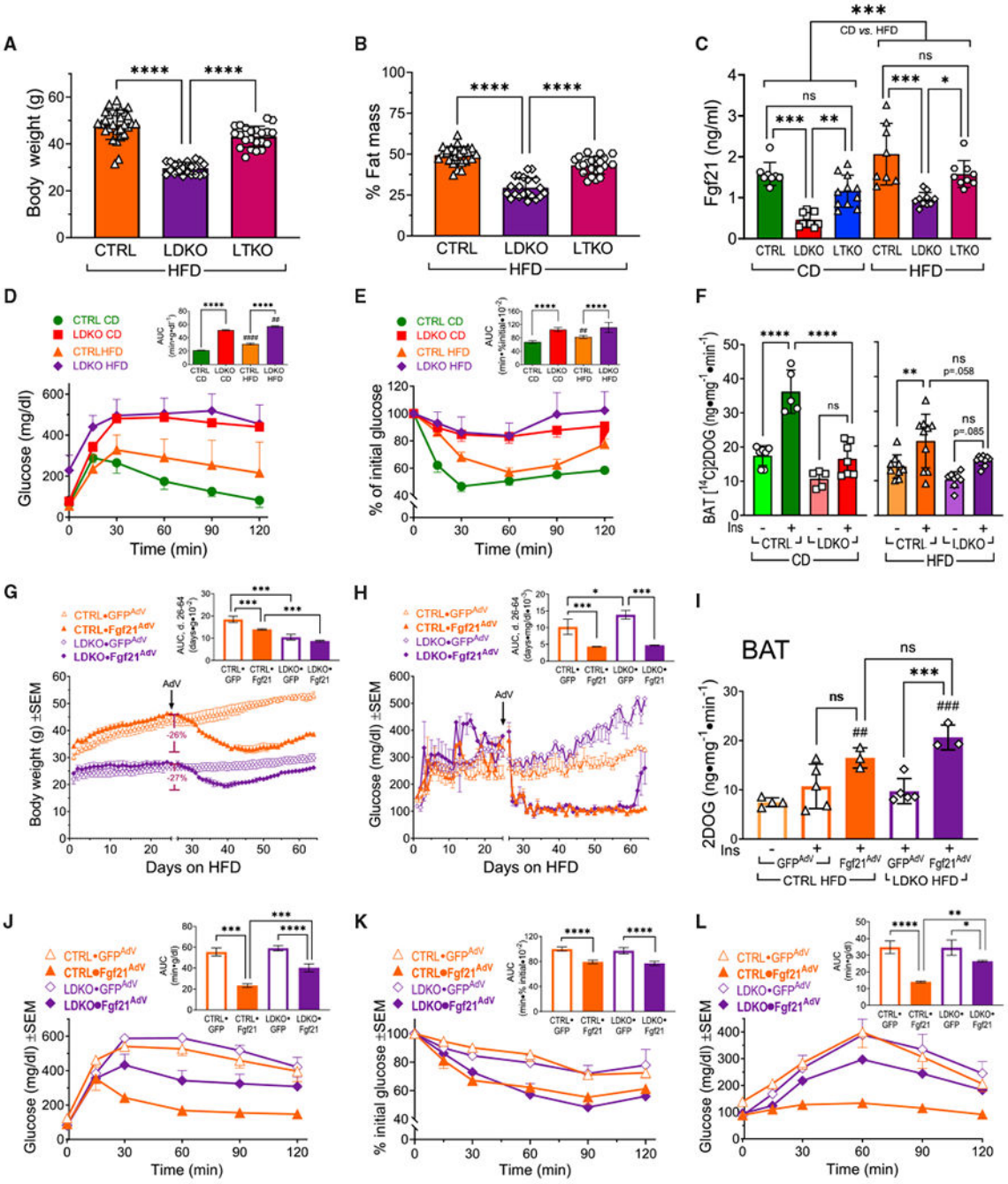

Figure 4. Exogenous Fgf21 reduces weight and blood glucose in high-fat-diet-fed LDKO mice without correcting hepatic glucose production

(A and B) Body weights (A) and DEXA-determined adipose mass (B; as a percentage of body weight) in 24-week-old male CTRL, LDKO, and LTKO mice fed a high fat diet (HFD) (n = 28, 21, and 22 mice).

(C) Serum Fgf21 concentration in fasted 14-week-old mice fed standard chow diet (CD) or HFD (from left to right: n = 8, 8, 10, 10, 11, or 9 mice).(D and E) Glucose homeostasis in 12- to 13-week-old male mice fed CD or HFD, assessed by (D) glucose tolerance (n = 10, 9, 10, and 10 mice) and (E) insulin tolerance tests (n = 10 mice per group). Inset graphs show

areas under curves; ##p < 0.01 and ####p < 0.0001 for HFD- versus CD-fed mice of same genotype.

(F) Basal and insulin-stimulated uptake of [^{14}C]2DOG into BAT of 14-week-old male mice fed CD (n = 7, 5, 5, and 7 mice) or HFD (n = 9, 10, 8, and 9 mice). Significance was assessed within each diet.

(G) Body weights of male HFD-fed CTRL and LDKO mice before and after infection with GFP^{AdV} or Fgf21^{AdV} (n = 5, 3, 5, and 3 mice). Vertical brackets denote equivalent mean weight loss (−26% or −27%) in CTRL and LDKO mice after infection with Fgf21^{AdV}. Inset graph shows AUCs in the post-infection period.

(H) Fed (afternoon) blood glucose concentrations of mice shown in (G). Inset graph shows AUCs in the post-infection period.

(I) Basal and/or insulin-stimulated uptake of [^{14}C]2DOG into BAT of HFD-fed CTRL and LDKO male mice 15 days after infection with GFP^{AdV}or Fgf21^{AdV} (n = 4, 5, 3, 5, and 3 mice); ##p < 0.01 and ###p < 0.001 versus CTRL·GFP^{AdV} mice in basal condition.

(J and K) Glucose homeostasis in HFD-fed CTRL and LDKO male mice infected with GFP^{AdV} or Fgf21^{AdV}, assessed by (J) GTT and (K) ITT assays performed 20 or 10 days after infection, respectively (n = 5, 3, 5, and 3 mice). Inset graphs show AUCs.

(L) Pyruvate tolerance test of HGP in HFD-fed CTRL and LDKO mice30 days after infection with GFP^{AdV} or Fgf21^{AdV} (n = 5, 3, 5, and 3 mice). Inset graph shows areas under glucose excursion curves.

Except for line graphs in (G), (H), (J), and (K) (mean ± SEM), lines or bars and error bars represent mean values ± SD. Differences between means were assessed with one-way ANOVA (A, B, and D–L) or 2 × 3 factorial ANOVA (C) followed by Tukey's HSD-based comparison of each group to every other: *p < 0.05; **p < 0.01; ***p < 0.001; ****p < 0.0001 between indicated groups. Additional significant differences (# symbol) are described in (D), (E) and (I).

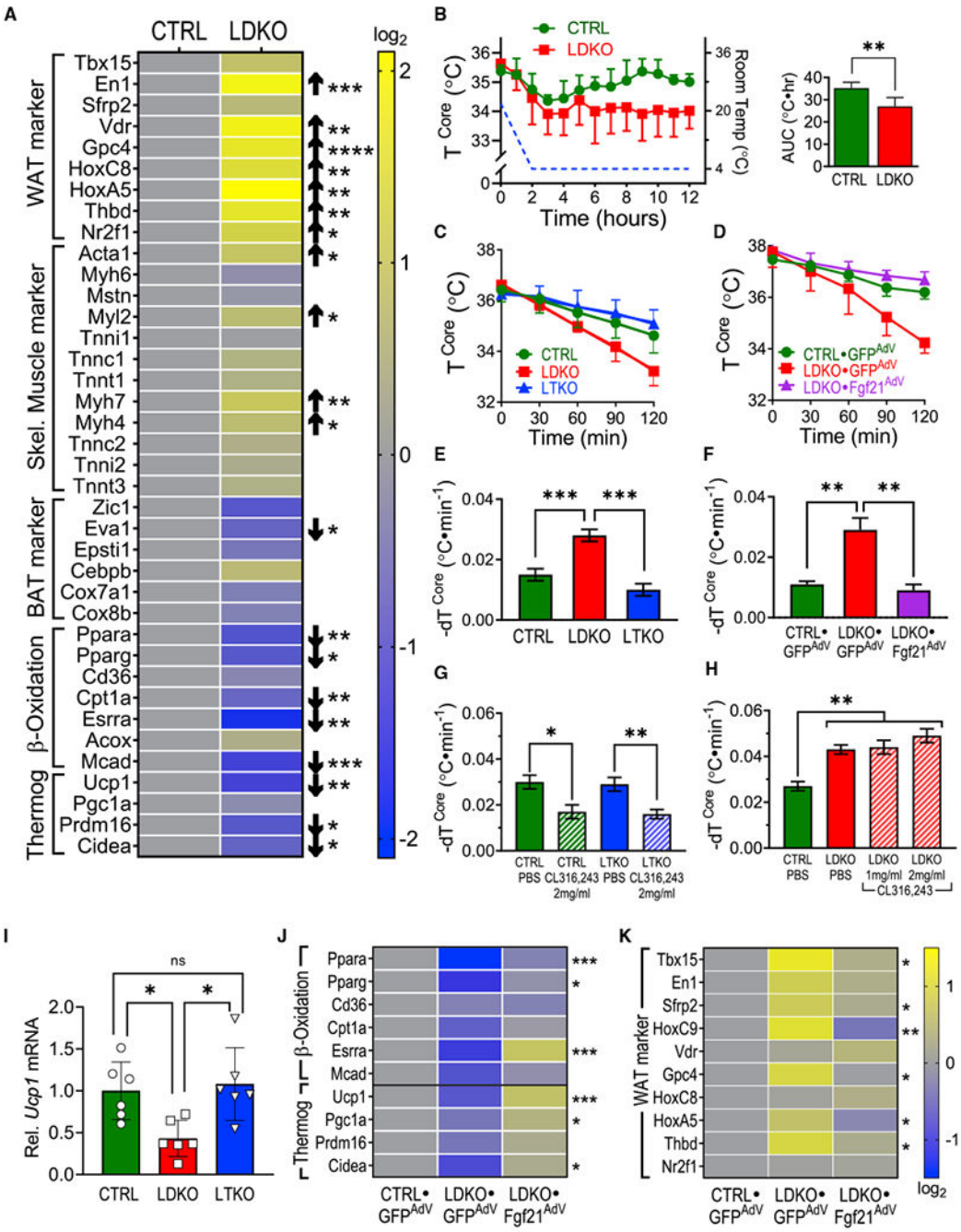

Figure 5. Cold intolerance and dysregulated BAT gene expression in LDKO mice are alleviated by restoration of hepatic Fgf21 expression

(A) qRT-PCR-based comparison of BAT gene expression in 12-week-old CTRL and LDKO mice (n = 6 and 6). Heatmap shows mean expression of genes characteristic of WAT, skeletal muscle, or BAT and of genes involved in fatty acid β-oxidation or thermogenesis. Color scale shows $\log_2$ fold change versus CTRL BAT. Gene-specific p values are indicated.

(B) Body core temperature (T^{Core}) versus room temperature (right-hand scale) of 14-week-old male CTRL and LDKO mice (n = 6 and 6) during chronic cold exposure. Mice were housed below thermoneutrality (22°C) for 3 days before the experiment. During the first 2

h, room temperature was reduced from 22°C to 4°C (dash line). Graph at right shows areas under T^{Core} curves.

(C) T^{Core} during acute exposure to 4°C cold in 14-week-old male CTRL, LDKO, and LTKO mice (n = 8, 6, and 7 mice).

(D) T^{Core} during acute exposure to 4°C cold in 12-week-old male CTRL and LDKO mice 12 days after infection of the liver with GFP^{AdV} or $Fgf21^{AdV}$ (n = 3 mice per group).

(E and F) Negative rate of change in mouse core temperature ($-dT^{Core}$; °C/min) during acute cold exposure, derived from linear regression of T^{Core} data in (C) and (D).

(G) Negative rate of change in T^{Core} ($-dT^{Core}$; °C/min) during acute cold exposure in 14-week-old male CTRL and LTKO mice (n = 5 mice per group). The mice were injected with β3 adrenergic receptor agonist CL316,243 (2 mg/mL) or vehicle (PBS) 1 h before transfer to 4°C (T^{Core} data used to fit dT are in Figure S5C).

(H) Negative rate of change in T^{Core} ($-dT^{Core}$; °C/min) during acute cold exposure in 14-week-old male CTRL and LDKO mice (n = 5 mice per group). The mice were injected with β3 adrenergic receptor agonist CL316,243 (1 or 2 mg/mL) or vehicle (PBS) 1 h before transfer to 4°C (T^{Core} data used to fit dT are in Figure S5D).

(I) Relative *Ucp1* mRNA expression in BAT of 14-week-old CTRL, LDKO, and LTKO male mice (n = 6 mice per group). Data are normalized by the CTRL mean.

(J and K) Relative BAT mRNA expression of (J) fatty acid β-oxidation and thermogenic genes (n = 5–7 mice/group) or (K) WAT marker genes (n = 8 mice/group) in 14-week-old male mice 12 days after infection with GFP^{AdV} or $Fgf21^{AdV}$. Color scale shows $\log_2$ fold change versus CTRL BAT. Significant differences are indicated for LDKO·GFP^{AdV} versus LDKO·$Fgf21^{AdV}$ mice.

Except for $-dT^{Core}$ data in (E)–(H) (mean ± SEM), lines or bars and error bars represent mean values ± SD. Differences between means were assessed by unpaired t tests (A, B, J, and K) or by one-way ANOVA (C–I) followed by Tukey's HSD-based comparison of each group to every other: *$p < 0.05$; **$p < 0.01$; ***$p < 0.001$; ****$p < 0.0001$ between indicated groups.